

¹ Crustal earthquakes in the Cook Inlet and Susitna region of southern Alaska

² Vipul Silwal^a, Carl Tape^a, Anthony Lomax^b

³ ^a*Geophysical Institute, University of Alaska, Fairbanks, USA*

⁴ ^b*ALomax scientific, Mouans-Sartoux, France*

⁵ **Abstract**

Several large ($M \geq 6$) earthquakes have occurred in the vicinity of Anchorage, Alaska, within the past century. The presence of the underlying subducting Pacific plate makes it difficult to determine the origin of these older earthquakes as either crustal, slab, or the subduction plate interface. We perform a seismological study of historical and modern earthquakes within the Cook Inlet and Susitna region, west of Anchorage. We first estimate hypocenters for historical large earthquakes in order to assess their likelihood of origin as crustal, slab, or plate interface. We then examine modern crustal seismicity to better understand the style of faulting and the location of active structures, including within (and beneath) the Cook Inlet and Susitna basins. We perform double-couple moment tensor inversions using high frequency body waves (1–10 Hz) for small to moderate ($M \geq 2.5$) crustal earthquakes (depth ≤ 30 km) occurring from 2007 to 2017. Our misfit function combines both waveforms differences as well as first-motion polarities in order to obtain reliable moment tensor solutions. The three focus regions—Beluga, upper Cook Inlet, and Susitna—exhibit predominantly thrust mechanisms for crustal earthquakes, indicating an overall compressive regime within the crust that is approximately consistent with the direction of plate convergence. Mechanisms within upper Cook Inlet have strike directions aligned with active anticlines previously identified in Cook Inlet from active-source seismic data. Our catalog of moment tensors is helpful for identifying and characterizing subsurface faults from seismic lineaments and from faults inferred from subsurface images from active-source seismic data.

⁶ **1. Introduction**

⁷ Modern tectonic activity in south-central Alaska is governed primarily by the northwestern subduction
⁸ of the Pacific plate beneath the North America plate (Figure 1). This setting is one of the most seismically
⁹ active regions in the world, having produced the M_w 9.2 1964 earthquake. It includes pervasive earthquakes
¹⁰ in the subducting slab, down to depths of 200 km, as well as crustal seismicity spanning a broad zone of
¹¹ intraplate deformation (Figure 2) [1, 2]. Many of the earthquakes—both large and small—are not clearly

Email addresses: vsilwal@alaska.edu (Vipul Silwal), ctape@alaska.edu (Carl Tape), anthony@alomax.net (Anthony Lomax)

12 associated with any faults that appear on published surface geological maps. With improved locations of
13 earthquakes and determination of the style of faulting from these earthquakes, we can better characterize
14 the extent, and activity, of faults in the region. Here we perform a seismological study of a tectonically
15 complex region of south-central Alaska to improve our understanding of active tectonics and seismic hazards
16 in the region.

17 The Pacific plate subducts to the northwest under south-central Alaska (Figure 1a). Attached to the
18 Pacific plate to the east is the Yakutat microplate, identified as an oceanic plateau, that is colliding and
19 subducting beneath Alaska [3, 4, 5]. The subducting Pacific/Yakutat plate is interpreted to be responsible
20 for the extremely shallow angle of subduction ($< 5^\circ$), far inland, as well as for the noteworthy lack of
21 volcanism in the Susitna basin and Talkeetna Mountains, in a magmatic gap between the Aleutian volcanic
22 arc on the west and the Wrangell volcanic field on the east (Figure 1a) [4, 6].

23 We focus on a lowlands region marked by the presence of two major sedimentary basins (Figure 1b and
24 Figure 3): the Cook Inlet basin south of the Castle Mountain fault, and the Susitna basin north of the
25 fault (Figure 1b). We refer to this region, which is outlined in Figure 1b, as the Cook Inlet and Susitna
26 region. The Susitna basin and the smaller, Peters Hill (or Yentna) basin [7, 8], are within the Susitna
27 lowlands, which is outlined in Figure 1b by [9]. The Susitna lowlands and the Cook Inlet basin (Figure 3)
28 are surrounded by mountains (Figure 1b): the Talkeetna Mountains to the east, the Alaska Range to the
29 northwest, the Tordillo Mountains to the west, and the Kenai Mountains to the south.

30 The Cook Inlet and Susitna region spans the western margin of the Pacific/Yakutat plate (Figure 1a) and
31 contains several notable tectonic elements. Contours of the depth to the top of the subducting Pacific plate
32 (i.e., the subduction interface) [10] show a clear kink from a westward-dipping slab to a northwestern-dipping
33 slab [11] (Figure 1a). The subduction interface ranges from a depth of 40 km in the southeast, beneath the
34 Kenai peninsula, to a depth of 100 km in the northwest, beneath the Alaska Range. The southeast corner of
35 the region also marks the approximate downdip extent of the 1964 M_w 9.2 earthquake (Figure 1a) [12, 13].
36 Slow slip and tectonic tremor have been identified on the deeper sections of the subduction interface, from
37 about 40 km to 80 km [14, 15, 16, 17]. The crustal thickness inferred from receiver functions is \sim 30 km in the
38 northern region [18], implying that these deeper slow slip events would arise from contact with subcrustal
39 mantle.

40 The dynamics of underlying subduction provide context for characterizing crustal structures and crustal
41 earthquakes, which are the target of this study. Within the Cook Inlet and Susitna region are two active
42 faults in the publication of [19]: the Pass Creek fault and the Castle Mountain fault. The earliest description
43 of the Pass Creek fault (PCF) appears in [20], who reported “over 2,000 feet” (p. 31) of displacement across
44 the fault. Using interferometric synthetic aperture radar (IFSAR) elevation data, [8] inferred the PCF to
45 be a northwest dipping normal fault and that it “appears likely that the scarp is a result of at least several
46 surface-rupturing earthquakes” (p. 1471). They estimated the fault has a slip-rate of \sim 0.5mm/yr and has

47 the potential of producing a $M_{\text{w}} = 6.9 \pm 0.3$ earthquake if the complete 37 km of the fault plane ruptured. [21]
48 discussed a possible interpretation for the Pass Creek fault as “north-directed backthrusting and hanging
49 wall extension above a blind, north-dipping master thrust” (p. 23).

50 The Castle Mountain–Lake Clark fault system extends 500 km from Lake Clark in the southwest to the
51 Talkeetna Mountains in the northeast [22]. The fault has been interpreted as a right-lateral strike-slip fault
52 based on geological features [22, 23, 24, 25, 26]. Two modern earthquakes, each well-recorded by regional
53 stations, provide support for the Castle Mountain fault—or at least the eastern portion—as a right-lateral
54 strike-slip fault. These earthquakes occurred just east of the Cook Inlet and Susitna region, as 1984-08-14
55 $M_{\text{w}} 5.8$ (depth 15 km) and 1996-11-11 $M_{\text{l}} 4.6$ (depth 17 km). A detailed study of the 1984 earthquake was
56 presented in [27]; this was the largest earthquake on the Castle Mountain–Lake Clark fault system within
57 the past 40 years [28, 29].

58 Recent analyses of the Castle Mountain fault have documented geomorphic features (e.g., scarps) con-
59 sistent with reverse slip across the fault, as well as a lack of definitive lateral offset indicators [21]. The
60 part of the CMF that extends across the Susitna lowlands is the only part of the fault that shows evidence
61 of Holocene displacement, based on geomorphic evidence [19]. This activity is supported by paleoseismic
62 evidence. [30] used data from nine trenches along the fault near Houston, Alaska. They identified four
63 major earthquakes in the past 2800 years, indicating a recurrence interval of ~ 700 years. Trenching results
64 from [31] suggested recurrence intervals closer to thousands of years. The two largest historical earthquakes
65 in the region, in 1933 and 1943, appear to have occurred near, but not on, the fault [32]. Additional faults
66 and folds, besides Pass Creek fault and Castle Mountain fault, have been inferred from potential field data
67 or identified within 3D active-source seismic data in Cook Inlet basin [33, 34, 35, 36, 26] and Susitna basin
68 [37, 38, 8] (Figure 1b).

69 We conduct a seismological study that spans three different methods and three sets of earthquakes
70 in the Cook Inlet and Susitna region (Table 1). First, in Section 2 we estimate the hypocenters of the
71 largest earthquakes ($M_{\text{w}} \geq 5.8$) that have occurred since the start of the instrumental era in 1904 [39]. We
72 use globally recorded arrival times of P and S waves, in addition to traveltimes predictions in a spherically
73 symmetric Earth model, within a probabilistic inversion for hypocenter and origin time. Second, in Section 3
74 we use P waveforms and first-motion polarities to estimate focal mechanisms for crustal earthquakes $M_{\text{w}} \geq$
75 2.5. This procedure is challenging on account of the lack of large earthquakes that are available. Third,
76 in Section 4 we relocate seismicity ($M \geq 1.5$, 1990–2017) using arrival time data and a double-difference
77 relocation algorithm [40]. The results from these three analyses reveal a predominance of thrust faulting
78 in the crust, consistent with structural inferences from subsurface images, but differing from the strike-slip
79 mechanisms previously estimated from the large historical earthquakes. Widespread seismicity and different
80 styles of faulting provide challenges for characterizing different scenarios for future large earthquakes in this
81 region.

82 **2. Hypocenter estimation of historical earthquakes**

83 At least 12 major earthquakes ($M_w \geq 5.8$) have occurred in the Cook Inlet and Susitna region since the
84 start of the instrumental era in 1904. Table 2 summarizes previous publications of the magnitudes for these
85 earthquakes. For larger earthquakes we use the Global Centroid Moment Tensor (GCMT) catalog [28, 29]
86 for events since 1976 and the ISC-GEM catalog [41, 42] for events before 1976. The ISC-GEM catalog
87 provides relocated hypocenters [43, 44] and magnitude estimates [45]. In recent years, it has expanded its
88 coverage of historical earthquakes to lower magnitudes. Doser and colleagues have estimated hypocenters,
89 magnitudes, and mechanisms for many historical earthquakes in south-central Alaska [32, 46, 47, 48].

90 Depth estimates of the hypocenters and of the subduction interface provide a starting point for interpreting
91 the earthquakes as either crustal, interface, or intraslab. Table 3 reveals a mix of crustal and intraslab
92 (or interface) earthquakes. Interestingly, the occurrence of earthquakes in the crust versus the slab appears
93 to have changed with time, as shown in Figure 4. Prior to 1950 most earthquakes were crustal; after 1950
94 all four earthquakes were in the slab. This pattern was previously noted [32] and is apparent over a larger
95 region. [32] speculated that stress changes from the 1964 $M_w 9.2$ earthquake were responsible for the shift
96 from crustal to slab earthquakes.

97 We use a nonlinear probabilistic approach to estimate the hypocenters of the 11 pre-1976 earthquakes
98 $M_w \geq 5.8$ in the region (Table 2). The code, NonLinLoc, uses an efficient global sampling algorithm to
99 obtain an estimate of the probability density function (pdf) in 3D space for the hypocenter location [49].
100 The pdf (and the likelihood) is computed using the misfit between the observed and theoretical arrival
101 times for teleseismic stations. Theoretical travel times are computed for a spherical earth with the ak135
102 velocity model [50] using the TauP Toolkit [51]. Recorded arrival times are obtained from the International
103 Seismological Centre [52].

104 Our full results for all 11 historical earthquakes are presented in [53]; next we highlight three of the
105 largest earthquakes.

106 *2.1. The 1933, 1943, and 1954 earthquakes*

107 We present results from three $M_w > 6$ earthquakes in the Cook Inlet and Susitna region: 1933-04-27
108 $M_w 6.8$, 1943-11-03 $M_w 7.3$, and 1954-10-03 $M_w 6.4$ (Table 2). These earthquakes were widely felt across
109 south-central Alaska, including Kodiak, to the southwest, and at least as far north as Fairbanks, which
110 is about 400 km from the epicenters. Section Appendix A summarizes felt reports of these earthquakes.
111 The 1933 earthquake toppled telegraph lines around Anchorage, broke storefront windows in Anchorage,
112 and shook houses off foundations in Old Tyonek. The 1954 earthquake produced minor landslides over
113 the highway, damaged a section of railroad, and damaged structures in Anchorage and the western Kenai
114 peninsula. Although having the largest magnitude of the three earthquakes, the 1943 earthquake did not lead

115 to any reported damage in the region. By comparison, the maximum shaking intensities in Anchorage—
116 which is approximately equidistant from the three earthquakes—were Modified Mercalli Intensity scale
117 (MMI; [54]) 6 (1933), MMI 5 (1943), and MMI 8 (1954) (Section Appendix A; [55]). These discrepancies
118 could arise from differences in source-to-site distances, from influences of 3D structure on ground motion,
119 from source effects (radiation pattern or directivity), and from possible inconsistencies in the MMI values
120 (e.g., are the MMI values from the same place in Anchorage?).

121 The seismicity cross sections in Figure 2b-c provide context for these three earthquakes. The plots show
122 our maximum likelihood (MLL) hypocenters for the three earthquakes in the context of modern seismicity
123 and estimated subsurface interfaces (subduction and Moho). From these results alone, it appears that the
124 1933 and 1943 earthquakes are crustal, while the 1954 earthquake was likely intraslab, though we cannot
125 rule out the subduction interface as a possibility (Table 3). We discuss this further in Section 5.3.

126 Station coverage and traveltimes residuals for our MLL hypocenters (and origin times) are shown in
127 Figure 5. The solution to the relocation problem is a posterior probability density function that can be
128 conveniently represented by samples—the posterior hypocenters—of the distribution [56]. Figure 6 shows our
129 posterior epicenters for the three earthquakes. These ‘clouds’ of posterior epicenters convey the uncertainty
130 associated with the epicenter estimation; in our cases, the clouds are approximately 30 km by 40 km. For each
131 posterior hypocenter we calculate its vertical distance to the subduction interface, and these differences are
132 then plotted as histograms in the bottom row of Figure 7. These distributions provide critical uncertainties
133 for the interpretation of the earthquakes as crustal, subduction interface, or intraslab. For example, the
134 estimated hypocenter depth shown in Figure 7c (bottom) is consistent with an intraslab origin for the 1954
135 earthquake. (However, note that we do not have uncertainties for the subduction geometry models, including
136 the one we have chosen to use [10]).

137 3. Moment tensor inversions for modern crustal earthquakes

138 Recorded seismograms can be used to characterize the style of faulting for an earthquake by using the
139 estimation method of moment tensor inversion. A double couple moment tensor is a 3×3 symmetric
140 matrix M whose eigenvalues are $\Lambda = (\lambda, 0, -\lambda)$. The seismic moment of a moment tensor is given by
141 $M_0 = \|M\|/\sqrt{2} = \|\Lambda\|/\sqrt{2}$, so for a double couple, $M_0 = \lambda$. We are concerned with estimating the
142 magnitude and orientation of the moment tensor. The strike, dip, and rake angles define the moment tensor
143 orientation, as well as one of the two possible fault planes. The moment tensor orientation can be described
144 as a ‘fault-plane solution’ or ‘focal mechanism’ or ‘source mechanism’; these terms do not encompass the
145 seismic moment (or magnitude). Seismologists represent double-couple moment tensors by plotting the sign
146 of the radial component of the displacement field at the source, then projecting it onto the lower hemisphere.
147 The two-colored pattern is a four-quadrant sphere that resembles a beachball; we use the term beachball

148 when referring to the plotting symbol.

149 Three catalogs of moment tensors are summarized in Figure 8: (a) [32]: large $M_w > 6$ historical (pre-
150 1964) earthquakes; (b) the GCMT catalog [28, 29]: post-1976 earthquakes, predominantly $M_w > 5.3$;
151 (c) crustal earthquakes from the Alaska Earthquake Center fault-plane catalog: predominantly $M_I > 3$. We
152 also considered the focal mechanism catalog of [10], which includes 117 earthquakes over a one-year period
153 of the MOOS deployment (2007–8). Almost all of these earthquakes are within the slab or to the southeast
154 of our focus region.

155 Within the Cook Inlet and Susitna region, we observe two historical crustal earthquakes (1933, 1943)
156 and zero crustal earthquakes since 1976 (GCMT: [28, 29]). There is one event in the GCMT catalog that is
157 ≤ 30 km depth, plotted as a red beachball near Anchorage in Figure 8b. The depth is listed as 15 km in the
158 GCMT catalog, but the Alaska Earthquake Center (AEC) earthquake catalog, using all available regional
159 data, lists 31 km for the depth, which would likely be an intraslab origin (not crustal) for the earthquake.
160 The GCMT magnitude of $M_w 5.3$ is near the completeness level for the catalog, which indicates that there
161 is limited global data for estimating the moment tensor. This might explain the large discrepancy between
162 the moment tensor from GCMT and the one from the Alaska Earthquake Center, as shown in Figure 6.

163 Focal mechanisms for crustal earthquakes since 1990 are available from Alaska Earthquake Center. The
164 mechanisms are estimated from first-motion polarities, and they vary widely across the region. Our primary
165 motivation was to use enhanced methods, including waveforms, and enhanced station coverage from the
166 past decade, to estimate moment tensors.

167 3.1. Event selection for moment tensor inversions

168 We consider earthquakes in the Cook Inlet and Susitna region shallower than 30 km and occurring
169 between 2007–08–15 and 2017–01–01. From the spatial distribution of crustal seismicity (Figure S11), we
170 identified three subregions to select events for moment tensor inversions: Beluga region, upper Cook Inlet
171 region, and Susitna region (Table 1 and Figure S9). The time period of event selection, 2007–2017, spans
172 two seismic experiments in the region: MOOS (2007–2009) [10, 57] and SALMON (2015–2017) [58, 59] and
173 also includes new stations from the EarthScope Transportable Array (TA) in Alaska (2014–2019). Station
174 coverage is a primary factor on the reliability of our moment tensor solutions. Events in 2010, following the
175 end of MOOS, have poor station coverage. Events starting in 2015 have the best coverage due to SALMON
176 and TA networks.

177 We selected 53 events for moment tensor inversions: 9 from the Beluga region, 22 from the upper Cook
178 Inlet region, and 22 from the Susitna region. Hypocenters and origin times were obtained from the AEC
179 catalog. These were fixed for the moment tensor inversions. Analyst-reviewed P arrival times and polarities
180 were used for stations in the permanent network (AK, AT, AV). For stations in temporary networks (MOOS,
181 SALMON, TA), we picked the P arrival times and assigned polarities.

182 *3.2. Moment tensor inversion method*

183 Estimating a moment tensor for an earthquake involves comparing observed waveforms with synthetic
184 waveforms calculated for an assumed moment tensor for an assumed model of Earth structure. We use the
185 same layered seismic velocity model used by the Alaska Earthquake Center for moment tensor inversions
186 and for locating earthquakes; see Table S1 of [60]. We use the ‘cut-and-paste’ approach to estimate moment
187 tensors for earthquakes [61, 62, 63]. In this approach, each three-component seismogram is cut into two body
188 wave windows and three surface wave windows. Different bandpass filters are applied to the body waves and
189 surface waves. The same procedures are applied to synthetic seismograms, which are then quantitatively
190 compared with the recorded seismograms, via a misfit function. As demonstrated in [60], the choices within
191 the misfit function can have a significant impact on the estimated best-fitting moment tensor. Our previous
192 studies [60, 64] employed a simplified treatment of first-motion polarities that is generalized here.

193 Within the grid-search moment tensor inversion, the synthetic seismograms are aligned with the observed
194 seismograms by applying time shifts to the synthetic waveforms that minimize the misfit between synthetic
195 and observed waveforms. In many cases, this minimization can result in time shifts that are unreasonable,
196 based on comparisons with a larger set of measurements. In these cases of cycle skipping, the synthetic
197 waveforms are aligned on the wrong portion of the observed waveforms. The challenges of cycle-skipping
198 and time shifts have been discussed previously [64, 65]. In our study we specify the observed P onset times,
199 which effectively eliminates the need for time shifts.

200 Figure 9 shows a moment tensor inversion result for one of 22 crustal earthquakes in the Susitna region.
201 Its relatively large magnitude (M_w 4.2) allows us to use surface waves, in addition to body waves. For
202 all the other events, only P waves (and P polarities) were used. The example shows the basic approach to
203 comparing recorded waveforms (black) with synthetic waveforms (red) generated using a layered Earth model
204 and a moment tensor source. Significant differences in shapes between data and synthetics are attributed
205 to complexities in 3D Earth structure that are not modeled by the synthetics. For this event, the recorded
206 waveforms to the southwest are influenced by Cook Inlet basin, as well as by Susitna basin from the source
207 region. Some of these differences in structure between our assumed 1D model and real 3D Earth structure
208 are encapsulated by the time shift maps shown in Figure 9.

209 *3.3. Misfit function*

210 Small earthquakes ($M_w < 3.5$) do not produce large signals at low frequencies. Therefore we are forced
211 to use higher frequency waveforms, which are sensitive to 3D structural heterogeneities. Most regional
212 networks do not have enough stations to capture the detailed effects of 3D structure on the wavefield. As
213 used in previous studies [66, 67, 68, 69], first-motion polarity measurements (i.e., up or down) can be used
214 to stabilize the waveform misfit function. Below we define our misfit function that combines waveforms
215 differences and polarity differences.

The L1-norm waveform misfit is given by

$$\Phi_w(M) = \sum_{j=1}^{N_s} \sum_{i=1}^5 \left[(\mathbf{u}_{ij} - \mathbf{s}_{ij}(M))^T \mathbf{W}_{ij} (\mathbf{u}_{ij} - \mathbf{s}_{ij}(M)) \right]^{1/2} \quad (1)$$

where N_s is the number of stations used, i is the window index for a seismogram, j is the station index for an event, \mathbf{u} is a discretized recorded seismogram, $\mathbf{s}(M)$ is a discretized synthetic seismogram for moment tensor M , \mathbf{W}_{ij} is a square weighting matrix with the same dimension as the number of time points. As discussed in Section S1, we choose \mathbf{W}_{ij} to be a constant-valued diagonal matrix with a weight factor that takes into account the duration of the time window, the width of the bandpass, and an optional user-specified weight. Recent approaches have considered non-diagonal weighting matrices based on estimated noise at each station [70, 71, 72].

The polarity misfit is given by

$$\Phi_p(M) = \frac{1}{2} \sum_{j=1}^{N_p} |p_j - t_j(M)| \quad (2)$$

where p is the observed polarity, t is the theoretical polarity for the moment tensor M , and N_p is the number of stations at which first-motion polarity is picked. p and t can either be +1 (up) or -1 (down). Considering the 1/2 factor, the polarity misfit for a station is either 0 or 1, and the allowable values for $\Phi_p(M)$ are $0, 1, \dots, N_p$.

The total misfit is a weighted sum of the normalized waveform and polarity misfit

$$\Phi(M) = h(N_s) \left(m \frac{\Phi_p(M)}{N_p} + (1-m) \frac{\Phi_w(M)}{\|\mathbf{u}\|_{L1}} \right) \quad (3)$$

where the waveform misfit normalization $\|\mathbf{u}\|_{L1}$ is same as given in equation 7 of [60], m is the weight given to the polarity misfit, and $h(N_s)$ is the station reward factor (see Section S1). Figure 10 shows the impact of using different weights for the polarity misfit on moment tensor solution. The Supporting Information includes text and figures to illustrate the roles of different variables in the misfit function. This misfit function was also used in [65, 73] for full moment tensor inversions.

3.4. Results

Our moment tensor inversion results for 53 crustal earthquakes in the three subregions (Table 1) are presented in Figure 11, in Tables S2–S4, and in [74]. The subregions exhibit predominantly thrust earthquake mechanisms that are consistent with the plate convergence direction of 339° (N21W) [2]. Specifically, the T axes of the mechanisms are near vertical, and the P axes of the mechanisms are near horizontal and point in the northwest direction of plate convergence.

In Figure 12 we compare our moment tensor results, which use P waveforms and first-motion polarities, with a catalog of mechanisms (AECfp) produced by the Alaska Earthquake Center that uses first-motion polarities only (fpfit: [75]). For the time period 2007-08-15 to 2017-01-01 and depths ≤ 30 km, the AECfp

catalog contains 46 earthquakes, 26 of which were examined in our study. The additional earthquakes in the AEC catalog were ones that were either not within our three subregions or were excluded by us due to low signal-to-noise levels for waveforms (Section 3.1). Therefore the comparison in Figure 12 is between a set of 53 moment tensors derived from P waveforms and a set of 46 derived from P polarities. The result in Figure 12a, which includes 27 that are not in (b), is a more coherent pattern of thrust faulting, whereas Figure 12b shows predominantly strike-slip faulting. This suggests that the inclusion of waveforms, as in our study, may help discriminate among strike-slip and thrust mechanisms in cases where P polarities alone cannot isolate the mechanism. Specifically, the moment tensor for a north-striking thrust fault dipping 45° (west or east) can be rotated 90° about its P-axis; this will result in a strike-slip moment tensor that is significantly overlapping with the original moment tensor (as quantified by $\omega = \angle(M_1, M_2) = 60^\circ$, which is much less than the maximum of 180°). Although the mechanisms look different, they are not easily constrained by seismic data, and a formal assessment of uncertainties could elucidate this point [60]. Of course, better station coverage would also help discriminate between the strike-slip and thrust mechanisms. By examining small, shallow earthquakes, we are unlikely to have the ray path coverage near the center of the focal sphere. For shallow events, the upward ray paths cover a small region of the Earth’s surface, where we are unlikely to have a station. For small events, the downward ray paths often have too-small of signal-to-noise ratios by the time they reach distant stations. Station coverage for the source mechanisms is best viewed in the beachball plots in [74].

4. Hypocenter relocation of modern crustal seismicity

We apply the double-difference hypocenter relocation method of [40] to crustal seismicity in the Cook Inlet and Susitna region. The double difference method relies on minimizing the difference between observed and theoretical travel-times for pairs of earthquakes at each station. The method, especially when used in conjunction with waveform cross correlations, has been effective in collapsing diffuse clouds of seismicity onto strikingly sharp fault-like features; meanwhile other diffuse clouds remain diffuse [76, 77]. The changes in the locations are also used to reduce the systematic errors due to the model, which could be used to improve the tomography models [78].

Our work expands on the results of [79], who relocated crustal earthquakes with $ml > 2.0$ and depths ≤ 50 km in southern Alaska occurring during 1988–1996 using the joint hypocenter determination (JHD) method [80]. They classified their results into five regions, one of which coincides with our target region: “Shallow North American intraplate earthquakes (0–25 km) located to the west of 149° W” (p. 96). Their results revealed diffuse seismicity within the crust.

We used a much larger data set, spanning from 1990-01-01 to 2017-01-01, and a more robust double-difference hypocenter relocation method [40]. We used crustal events (depth ≤ 30 km) with $M_l \geq 1.5$

274 occurring between 1990-01-01 and 2017-01-01 (Table 1). With these selection criteria, we started with 5726
275 events from the AEC catalog. The final relocated catalog, after removing 35 (depth > 40 km) events,
276 contained 4748 earthquakes. The changes between the initial hypocenter and final hypocenter are displayed
277 in Figures S14 and S13. The mean change in epicenter is about 5 km and the standard deviation of depth
278 changes is about 6 km.

279 In general, after relocation the diffuse seismicity remains diffuse (Figure 13). Similar results were obtained
280 for relocations in the Los Angeles basin by [76]. [76] explained the diffuse hypocenters as an effect of complex
281 3D brittle structure with interlaced strike-slip faults and thrust faults. The main lineament in our study
282 region, within the Beluga region, is rotated toward a N-S alignment after relocation (Figure 13). Future
283 efforts using new stations and waveform cross-correlation measurements could improve our results.

284 **5. Discussion**

285 Here we summarize our seismological results in the context of previous work within the three regions of
286 interest (Table 1). We then discuss implications for active faults and larger earthquakes in the region.

287 *5.1. Structures and active tectonics in the Cook Inlet and Susitna region*

288 *Beluga region*

289 The Beluga region (Figure 11a) is physiographically marked by a triangular-shaped feature which we
290 describe as the Beluga “interlowland region” (BILR), after [81]. The BILR comprises four small mountains,
291 each on the order of 1000 m in elevation: Mount Susitna, Little Mount Susitna, unnamed (south of Wolf
292 Lakes), and Beluga Mountain (Figure 11a). The BILR is bounded to the northeast by the Susitna basin
293 and the Beluga Mountain fault, to the south by Castle Mountain fault and the Cook Inlet basin, and to the
294 west by a north-south physiographic low that is the drainage for the Talachulitna river, which flows north.

295 The Beluga region (Figure 11a) contains a seismic lineament named the Talachulitna seismic zone (TSZ)
296 by [46]. The TSZ is approximately aligned with the western margin of the BILR, near the Talachulitna
297 river. [46] interpreted the TSZ to be dipping steeply to the northeast (their Fig. 4c). The scatter in their
298 results—and ours (Figure 11a)—prevents us from identifying any alignment with depth.

299 Earthquake mechanisms are challenging to estimate for the TSZ. [46] tabulated one focal mechanism
300 in this zone (AF2; their Table 2), from the AEC focal mechanism catalog, but the current AEC catalog
301 has only five events (Figure 12b), none of which pre-date 2005. We present moment tensors for 9 events,
302 all of which are shallower than 12 km (Table S2). The mechanisms have considerable variation, with a
303 predominance of thrust faulting consistent with east-west compression (Figure 11a).

304 Regional geophysical data and geological data provide context for the active seismicity. The BILR is
305 mainly composed of Cenozoic and Mesozoic intrusive and volcanic rocks [82, 83] that are adjacent to Cenozoic

306 sedimentary basins to the north (Susitna), west (Beluga), and south (Cook Inlet) (Figure 1b). [84] and [81]
307 used gravity data and magnetic data to identify the Beluga Mountain fault on the northern front of the
308 BILR as a thrust fault dipping southwest; however recent fault kinematic data do not support a thrust
309 interpretation [85]. The Beluga Mountain fault does not appear to be seismically active or connected with
310 the Talachulitna seismic zone.

311 Examining Figure 11a, we speculate that the Talachulitna seismic zone represents a north-striking, east-
312 dipping thrust fault system that may represent some weakness within the crustal block north of the Castle
313 Mountain fault and west of Susitna basin. This weakness, aligned with the western margin of the BILR,
314 could accommodate some regional compression and contribute to uplift of the BILR.

315 *upper Cook Inlet region*

316 Earthquakes in the upper Cook Inlet region occur beneath Cook Inlet basin, a large, long-lived forearc
317 sedimentary basin whose Cenozoic strata have a maximal thickness of 7.6 km and overlie a Mesozoic section
318 approximately 8 km thick [86, 87, 88]. The Cook Inlet basin is bounded by the Aleutian Range to west, the
319 Alaska Range and Talkeetna Mountains to the north, and the Kenai and Chugach Mountains to the east
320 (see Figure 1). On the north, the Castle Mountain Fault separates the Cook Inlet basin from the adjoining
321 Susitna basin. The similarities in structures of Cook Inlet and Susitna basins suggests that their histories
322 are linked [88].

323 The 22 events in our study (Figure 11b, Table S3) mostly have depths in the 10–20 km range, placing
324 them either within the Mesozoic strata or the crystalline basement. The crust within upper Cook Inlet
325 (north of West Foreland) is more seismically active than the lower Cook Inlet; this is possibly related to the
326 underlying subduction of the Yakutat microplate [4, 7].

327 Folds in Cook Inlet are complex, discontinuous structures with variable shape and vergence that probably
328 developed by right-transpressional deformation on oblique-slip faults extending downward into the Mesozoic
329 strata beneath the Cenozoic basin [35]. A discussion of the complex folding and faulting structures in the
330 basin can be found in [86, 26].

331 Our moment tensor inversions for 22 earthquakes reveal thrust fault mechanisms whose strike angles are
332 generally aligned with the Cook Inlet anticlines [35, 19] (Figure 11b). The simplest explanation is that the
333 anticline structures, identified within active-source seismic data, arise from NW–SE thrust faulting identified
334 from modern earthquakes.

335 *Susitna region*

336 The Susitna region exhibits diffuse seismicity with the larger earthquakes (22 in this study) exhibiting
337 thrust fault mechanisms (Figure 11c, Table S4). These mechanisms, with NW–SE P-axes, are consistent
338 with the convergence direction of N21W [2] between the Pacific and North America plates. They are also

339 consistent with the interpretation of subsurface contractional structures in the region [81]. Further work is
340 needed to relate the stresses within the crust to stresses arising from the subducting slab; such an effort
341 should take into account the microplate setting [89] and continuum mechanical modeling [e.g., 90, 91].

342 The earthquakes in the Susitna region occur within a tectonically complicated region. The region is
343 marked by the Susitna basin (Figure 3b) [9, 92], which is bounded by the Alaska Range to the north,
344 the Talkeetna Mountains to the east, the BILR (and Beluga Mountain fault) to the west, and the Castle
345 Mountain fault to the south. The crustal earthquakes are vertically bounded by the overlying Susitna basin
346 and the underlying subducting Pacific plate. The Pacific plate exhibits two transitions in this region: (1) a
347 kink in its geometry (e.g., Figure 6), from western dipping to more northwestern dipping [11] and (2) an
348 interpreted transition from normal subducting crust in the west to overthickened Pacific/Yakutat crust in
349 the east (Figure 1a). It is possible that either, or both, of these slab-related features contributes to the
350 concentration of crustal seismicity in the eastern part of the Susitna region.

351 Comparison between the crustal earthquakes and the basement surface (Figure S12c) reveals several
352 earthquakes below the deepest part of Susitna basin and within the uppermost 10 km. It is possible that
353 these earthquakes occur on deeper extensions of the structures mapped within the subsurface basin structures
354 [37, 8]. The diffuse seismicity in the eastern portion of the Susitna region underlies the shallowest portion of
355 the basin and are not associated with any previously identified subsurface structures. However, it is worth
356 noting that the lack of faults could be related to the lack of data, as no seismic reflection studies have been
357 done in the eastern part of the Susitna basin (east of the Susitna River), as far as we know.

358 5.2. Implications of minor earthquakes for active faults

359 From our perspective, seismic evidence for an active fault includes: (1) alignment of seismicity into
360 a lineament (2) occurrence of moment tensors with one of its two possible fault planes parallel to the
361 lineament, and (3) occurrence of large ($M \geq 6$) earthquakes. This seismic evidence should be assessed
362 alongside geological evidence, whether in the form of slip rates inferred from dated offset units at the
363 surface, from structural offsets inferred from seismic imaging and potential field data, and from paleoseismic
364 evidence of past large earthquakes [30, 19, 81, 21].

365 Our presentation in Figure 11 displays these three types of seismic evidence: relocated hypocenters of
366 modern earthquakes, source mechanisms for the largest modern earthquakes, and estimated epicenters of
367 the largest two historical earthquakes, in 1933 and 1943. We also superimpose previously published faults,
368 and here we discuss the possible connections between faults identified from surface and subsurface geological
369 data with seismic activity at depth.

370 Most of the relocated seismicity does not exhibit seismic lineaments (Section 4). The only lineament we
371 are confident about is the previously identified [46] Talachulitna seismic zone (Figure 11a). There is no fault
372 mapped near this lineament (Figure 11a). It is possible that this seismic zone is an expression of a single

fault, but the source mechanisms are variable, and there is no definitive evidence for hosting any moderate or large earthquake. To the northeast, within the Susitna region (Figure 11c), the seismicity is diffuse but the mechanisms are more consistent, exhibiting thrust faulting. Deformation within the crust appears to be broadly distributed, rather than concentrating on a few discrete faults. The same pattern is true to the south, within the upper Cook Inlet region (Figure 11c): diffuse seismicity with consistent thrust fault mechanisms. In both the Susitna region and the upper Cook Inlet region, there are subsurface fault and fold structures identified from modeling seismic reflection data and potential field data (gravity and magnetics). If these identified faults penetrate the basement rocks that underlie the sedimentary basin fill (Figure 3b), then it seems reasonable to ascribe the style of faulting inferred from the earthquake mechanisms to the style of faulting occurring near the surface. Therefore, on the basis of our results from small, recent earthquakes (Figure 11), we would ascribe thrust faulting to the active folds in Cook Inlet basin [35] and thrust faulting to the structures in Susitna basin [37, 8]. This is in contrast to the existing catalog of earthquake mechanisms, which favors strike-slip faulting in these regions (Figure 12b). With all evidence taken together—not just modern earthquakes—it is likely that a range of strike-slip, thrust, and oblique faulting is possible in Cook Inlet and Susitna region. See Figure 8 of [93] for a comparison of regional tectonic models.

5.3. Structures responsible for 1933, 1943, and 1954 earthquakes

Large earthquakes rupture along faults with dimensions of tens of kilometers. Previous studies of large sets of earthquakes provides scaling between magnitude and fault dimensions. Assuming a circular fault (radius r , fault dimension $2r$) and a stress drop between 0.2 MPa and 20 MPa [94], the corresponding fault dimension would be

- 15–70 km for the 1933 M_w 6.8 earthquake
- 27–125 km for the 1943 M_w 7.3 earthquake
- 10–44 km for the 1954 M_w 6.4 earthquake

The empirical relationships of [95] are also within these ranges. These dimensions should be kept in mind when examining Figures 6 and 11.

Our probabilistic hypocentral estimations for the 1933, 1943, and 1954 earthquakes (Figure 6, Section 2.1) provide a starting point for interpreting the structures responsible (and not responsible) for these earthquakes. The 1933 earthquake (Figure 6) occurred within the region of the concentration of modern earthquakes in the upper Cook Inlet region (Figure 11b). It seems possible that one of the northeast-striking thrust faults could have hosted the 1933 earthquake [35]. The 1943 earthquake (Figure 6) maximum likelihood epicenter is on the Beluga Mountain fault (L43 label in Figure 11c), yet the uncertainty region for the epicenter (Figure 6) also includes some of the north-striking faults in Susitna basin, as well as the Talachulitna seismic zone (Figure 11a). Therefore all of these faults are candidates for the 1943 earthquake.

406 Reliable source mechanisms for historical earthquakes would provide valuable constraints on the (un-
407 known) host faults. Here we summarize results, and challenges, from [32], who estimated source mechanisms
408 for the 1933, 1943, and 1954 earthquakes, among others. They used limited teleseismic data to estimate
409 the source mechanisms: P, PP, and S waveforms for 13 global stations, as well as first-motion polarities,
410 where available. (By comparison, there are >100 global stations providing arrival times used in Figures 6
411 and 5.) They present waveform comparisons for all events in their Figure A2, offering the reader the chance
412 to assess the reliability of the results. The numbers of stations and waveforms used for each event were
413 as follows: 3 stations (8 waveforms) for 1933, 5 stations (9 waveforms) for 1943, 6 stations (11 waveforms)
414 plus first-motion polarities for 1954. Surface waves were not used, though they provide stable constraints
415 for global moment tensor inversions [28, 96], mainly owing to the insensitivity of their long periods to 3D
416 structural heterogeneities in Earth.

417 The picture of faulting from the 1933 and 1943 mechanisms [32] is one of strike-slip faulting (Figure 6),
418 either right-lateral on a northeast-striking fault or left-lateral on a northwest-striking fault. Based on the
419 points above, and from our own experience examining moment tensor uncertainties with modern regional
420 earthquakes [60], we would advise caution in basing any interpretation on the historical mechanisms. For
421 example, rotation of these beachballs by 90° about their P-axes would lead to a north-striking thrust
422 fault that would satisfy some of the historical seismic waveforms and first-motion polarities. Our epicenter
423 locations for 1933 and 1943 earthquakes support the findings of [32] and exclude the Castle Mountain fault
424 as a source for the two earthquakes.

425 The 1954 earthquake likely occurred within the subducting Pacific plate, rather than on the subduction
426 interface or within the lower overriding crust. The depth distribution of modern seismicity in this region is
427 nearly continuous (Figure 7c, Figure 1b), making it challenging to discriminate among the three possibilities.
428 This event has the benefit of better data than the older events, and therefore the mechanism should be more
429 reliable. Two source mechanisms from previous studies are shown in Figure 6 and reveal strike-slip faulting,
430 not low-angle thrust faulting that would be expected for the subduction interface.

431 6. Summary

432 We present a seismological study of the tectonically complex region of Cook Inlet and Susitna, west of
433 Anchorage, Alaska (Figure 1), with emphasis on crustal earthquakes. Using arrival time data, we estimate
434 hypocenters of all 11 historical earthquakes $M_w \geq 5.8$ that have occurred in the Cook Inlet and Susitna
435 region. Using waveforms from modern earthquakes, we estimate source mechanisms for 53 crustal earth-
436 quakes (M_w 2.5 to 4.8). Using arrival time data, we relocate a catalog of 5726 earthquakes ($M_l \geq 1.5$). We
437 examine these seismological results in the context of regional tectonics, regional structures (basins, faults,
438 folds), and previously published source mechanisms of older (and larger) earthquakes.

439 Here we summarize our main findings:

- 440 1. Within the Cook Inlet and Susitna region, we can generalize the earthquake patterns into two time
441 periods (Figure 4). In the last several decades there have been small-magnitude thrust events in
442 the crust and larger events in the slab. Prior to 1950 or so there have been large-magnitude crustal
443 earthquakes that were possibly strike-slip.
- 444 The existence of two crustal earthquakes (1933 M_w 6.8 and 1943 M_w 7.3) motivates our examination
445 of modern crustal earthquakes and geological structures. Within our three focus regions (Figure 8, the
446 crust has not produced notable earthquakes in the recent decades of high-quality seismic data: there
447 are zero crustal earthquakes in the GCMT catalog ([28]: 1976–2018). (The 1984 and 1996 earthquakes
448 occurred to the east: Figure 6.)
- 449 2. Our source mechanisms favor an interpretation of thrust faulting (Figure 12a) over strike-slip faulting
450 (Figure 12b). Uncertainties in the source mechanisms are considerable, owing to the small magnitudes
451 (which limits the inclusion of surface waves) and the extreme crustal heterogeneity (notably basins:
452 Figure 3b), which was not accounted for in modeling synthetic seismograms.
- 453 3. Seismicity in the Susitna region (Figure 11c, Figure 13) is diffuse [79]. As discussed in Section 5.1, the
454 deforming crust in this region may be influenced by forces arising from subduction, either from the
455 underlying slab or from tractions of the flowing mantle [26, 82].
- 456 4. The 1933 M_w 6.8 earthquake occurred beneath Cook Inlet basin, in a region exhibiting northeast-
457 striking thrust fault source mechanisms (Figure 11b) that are aligned with the axes of active fold
458 anticlines [35]. It is possible that the 1933 earthquake ruptured as a thrust fault, though the previously
459 published source mechanism (using three stations) is a strike-slip mechanism. [35] suggested that a
460 fault-cored anticline within Cook Inlet could have hosted the 1933 earthquake, and [32] concurred,
461 though neither study ruled out the Castle Mountain fault as a source.
- 462 5. The 1943 M_w 7.3 Susitna earthquake is the fourth largest earthquake ever to occur in mainland Alaska,
463 following 1964 M_w 9.2 megathrust, 2002 M_w 7.9 Denali fault, and 1979 M_w 7.4 Wrangell–St. Elias.
464 Its hypocenter was beneath the Susitna basin, possibly on a structure associated with the Beluga
465 Mountain fault or the Talachulitna seismic zone (Figure 11a). A previous study used waveforms from
466 five stations [32] to estimate a strike-slip source mechanism for the earthquake (Figure 6). Moment
467 tensors of crustal events closest to the 1943 epicenter exhibit thrust mechanisms, consistent with
468 inferred subsurface structures [37, 81]. Either a strike-slip or a thrust fault seems most likely for the
469 1943 earthquake.
- 470 6. The 1954 M_w 6.4 earthquake beneath the Kenai peninsula was likely an intraslab earthquake. It pro-
471 duced the strongest shaking (MMI 8) ever documented on the western Kenai peninsula (Section Ap-
472 pendix A). The subducting Pacific plate has produced much larger intraslab earthquakes, such as the

473 deeper and more distant M_w 7.1 earthquake on 2016-01-24. For considering ground motion calculations
474 from potential earthquakes in the region (“scenario earthquakes”), it is worth considering a M_w 7.0
475 earthquake in the 1954 hypocentral region.

476 **7. Acknowledgments**

477 This project was supported by the Earthquakes Hazards Program of the United States Geological Survey,
478 Award G15AP00052. Our manuscript benefitted from reviews by Diane Doser and Richard Stanley and
479 feedback from Rich Koehler and Peter Haeussler. Digital files for faults in the Susitna basin region were
480 provided by Anjana Shah, Richard Stanley, and Peter Haeussler. Thanks to Lea Gardine for converting
481 digital fault files from GIS format to text format. Digital files for the basement surface of Susitna and
482 Peters Hill basins (Figure 3b) were provided by Jeff Phillips at USGS. We thank Domenico Di Giacomo of
483 the International Seismological Centre for providing arrival time data for six of the historical earthquakes
484 presented here and in [53]: 1929-07-03, 1933-06-12, 1933-06-13, 1933-06-19, 1936-10-23, 1937-10-24. We
485 thank Celso Alvizuri for code developments for data processing and moment tensor inversions.

486 **References**

- 487 [1] R. A. Page, N. N. Biswas, J. C. Lahr, H. Pulpan, Seismicity of continental Alaska, in: D. B. Slemmons, E. R. Engdahl,
488 M. D. Zoback, D. D. Blackwell (Eds.), Neotectonics of North America, The Geology of North America, Geol. Soc. Am.,
489 Boulder, Colo., USA, 1991, Ch. 4, pp. 47–68, Decade Map Volume 1.
- 490 [2] P. Bird, An updated digital model of plate boundaries, *Geochem. Geophys. Geosyst.* 4 (2003) 1–52.
491 doi:10.1029/2001GC000252.
- 492 [3] G. Plafker, T. L. Hudson, T. Bruns, M. Rubin, Late Quaternary offsets along the Fairweather fault and crustal plate
493 interactions in southern Alaska, *Can. J. Earth Sci.* 15 (5) (1978) 805–816.
- 494 [4] D. Eberhart-Phillips, D. H. Christensen, T. M. Brocher, R. Hansen, N. A. Ruppert, P. J. Haeussler, G. A. Abbers, Imaging
495 the transition from Aleutian subduction to Yakutat collision in central Alaska, with local earthquakes and active source
496 data, *J. Geophys. Res.* 111. doi:10.1029/2005JB004240.
- 497 [5] G. L. Christeson, S. P. S. Gulick, H. J. A. van Avendonk, L. L. Worthington, R. S. Reece, T. L. Pavlis, The Yakutat
498 terrane: Dramatic change in crustal thickness across the Transition fault, Alaska, *Geology* 38 (10) (2010) 895–898.
- 499 [6] S. Rondenay, L. G. J. Montési, G. A. Abbers, New geophysical insight into the origin of the Denali volcanic gap, *Geo-*
500 *phys. J. Int.* 182 (2010) 613–630.
- 501 [7] P. J. Haeussler, An overview of the neotectonics of interior Alaska: Far-field deformation from the Yakutat microplate
502 collision, in: J. T. Freymueller, P. J. Haeussler, R. Wesson, G. Ekström (Eds.), *Active Tectonics and Seismic Potential*
503 of Alaska, Vol. 179 of *Geophysical Monograph*, Am. Geophys. Un., Washington, D.C., 2008, pp. 83–108.
- 504 [8] P. J. Haeussler, R. W. Saltus, R. G. Stanley, N. Ruppert, K. Lewis, S. M. Karl, A. Bender, The Peters Hills basin,
505 a Neogene wedge-top basin on the Broad Pass thrust fault, south-central Alaska, *Geosphere* 13 (5) (2017) 1464–1488.
506 doi:10.1130/GES01487.1.
- 507 [9] C. E. Kirschner, Map Showing Sedimentary Basins of Onshore and Continental Shelf Areas, Alaska, U.S. Geol. Survey
508 Miscellaneous Investigation Series I-1873 (1988).

- 509 [10] J. Li, G. A. Abers, Y. Kim, D. Christensen, Alaska megathrust 1: Seismicity 43 years after the great 1964 Alaska
510 megathrust earthquake, *J. Geophys. Res.*118 (2013) 4861–4871. doi:10.1002/jgrb.50358.
- 511 [11] N. A. Ratchkovski, R. A. Hansen, New evidence for segmentation of the Alaska subduction zone, *Bull. Seis-
512 mol. Soc. Am.*92 (5) (2002) 1754–1765.
- 513 [12] J. Davies, L. Sykes, K. Jacob, Shumagin seismic gap, Alaska Peninsula: History of great earthquakes, tectonic setting,
514 and evidence for high seismic potential, *J. Geophys. Res.*86 (B5) (1981) 3821–3855.
- 515 [13] G. Ichinose, P. Somerville, H. K. Thio, R. Graves, D. O'Connell, Rupture process of the 1964 Prince William
516 Sound, Alaska, earthquake from the combined inversion of seismic, tsunami, and geodetic data, *J. Geophys. Res.*112.
517 doi:10.1029/2006JB004728.
- 518 [14] Y. Ohta, J. T. Freymueller, S. Hreinsdóttir, H. Suito, A large slow slip event and the depth of the seismogenic zone in
519 the south central Alaska subduction zone, *Earth Planet. Sci. Lett.*247 (2006) 108–116.
- 520 [15] M. Wei, J. J. McGuire, E. Richardson, A slow slip event in the south central Alaska Subduction Zone and related
521 seismicity anomaly, *Geophys. Res. Lett.*39. doi:10.1029/2012GL052351.
- 522 [16] Y. Fu, J. T. Freymueller, Repeated large Slow Slip Events at the south central Alaska subduction zone, *Earth Planet.
523 Sci. Lett.*375 (2013) 303–311.
- 524 [17] S. Li, J. Freymueller, R. McCaffrey, Slow slip events and time-dependent variations in locking beneath Lower Cook Inlet
525 of the Alaska-Aleutian subduction zone, *J. Geophys. Res. Solid Earth*121 (2016) 1060–1079. doi:10.1002/2015JB012491.
- 526 [18] E. Veenstra, D. H. Christensen, G. A. Abers, A. Ferris, Crustal thickness variation in south-central Alaska, *Geology*34 (9)
527 (2006) 781–784.
- 528 [19] R. D. Koehler, R.-E. Farrell, P. A. C. Burns, R. A. Combellick, Quaternary faults and folds in Alaska: A digital
529 database, *Alaska Div. Geol. Geophys. Surv. Miscellaneous Publication* 141, 31 p., 1 sheet, scale 1:3,700,000 (2012).
530 doi:10.14509/23944.
- 531 [20] S. R. Capps, The Yentna District Alaska, U.S. Geol. Survey Bulletin 534, Washington, D.C. (1913).
- 532 [21] R. D. Koehler, G. A. Carver.
- 533 [22] A. Grantz, Strike-Slip Faults in Alaska, 1966, U.S. Geol. Survey Open-File Report 66-53, Washington, D.C.
- 534 [23] P. J. Haeussler, R. W. Saltus, 26 km of offset on the Lake Clark fault since late Eocene time, in: P. J. Haeussler, J. P.
535 Galloway (Eds.), *Studies by the U.S. Geological Survey in Alaska*, 2004, U.S. Geol. Survey, Washington, D.C., 2005, pp.
536 1–4, Professional Paper 1709-A.
- 537 [24] J. M. Trop, D. A. Szuch, M. Rioux, R. B. Blodgett, Sedimentology and provenance of the Upper Jurassic Naknek
538 Formation, Talkeetna Mountains, Alaska: Bearings on the accretionary tectonic history of the Wrangellia composite
539 terrane, *Geol. Soc. Am. Bull.*117 (5/6) (2005) 570–588. doi:10.1130/B25575.1.
- 540 [25] J. B. Willis, P. J. Haeussler, R. L. Bruhn, G. C. Willis, Holocene slip rate for the western segment of the Castle Mountain
541 fault, Alaska, *Bull. Seismol. Soc. Am.*97 (3) (2007) 1019–1024. doi:10.1785/0120060109.
- 542 [26] P. J. Haeussler, R. W. Saltus, Location and extent of Tertiary structures in Cook Inlet basin, Alaska, and mantle dynamics
543 that focus deformation and subsidence, in: J. A. Dumoulin, J. P. Galloway (Eds.), *Studies by the U.S. Geological Survey*
544 in Alaska, 2008–2009, U.S. Geol. Survey, Washington, D.C., 2011, pp. 1–26, Professional Paper 1776-D.
- 545 [27] J. C. Lahr, P. A. Page, C. D. Stephens, K. A. Fogelman, Sutton, Alaska, earthquake of 1984: Evidence for activity on
546 the Talkeetna segment of the Castle Mountain fault system, *Bull. Seismol. Soc. Am.*76 (4) (1986) 967–983.
- 547 [28] A. Dziewonski, T.-A. Chou, J. H. Woodhouse, Determination of earthquake source parameters from waveform data for
548 studies of global and regional seismicity, *J. Geophys. Res.*86 (B4) (1981) 2825–2852. doi:10.1029/JB086iB04p02825.
- 549 [29] G. Ekström, M. Nettles, A. M. Dziewoński, The global GCMT project 2004–2010: Centroid-moment tensors for 13,017
550 earthquakes, *Phys. Earth Planet. Inter.*200-201 (2012) 1–9. doi:10.1016/j.pepi.2012.04.002.
- 551 [30] P. J. Haeussler, T. C. Best, C. F. Waythomas, Paleoseismology at high latitudes: Seismic disturbance of upper Quaternary

- 552 deposits along the Castle Mountain fault near Houston, Alaska, *Geol. Soc. Am.*114 (10) (2002) 1296–1310.
- 553 [31] R. D. Koehler, R. D. Reger, E. R. Spangler, A. I. Gould, Investigation of potentially active tectonic faults along the
554 route of the proposed Alaska Stand Alone Pipeline, Livengood to Cook Inlet, Alaska, *Alaska Div. Geol. Geophys. Surv.,*
555 Report of Investigation 2015-4, 71 p. (2015). doi:10.14509/29409.
- 556 [32] D. I. Doser, W. A. Brown, A study of historic earthquakes of the Prince William Sound, Alaska, Region, *Bull. Seis-
557 mol. Soc. Am.*91 (4) (2001) 842–857.
- 558 [33] L. B. Magoon, W. L. Adkison, R. M. Egbert, Map showing geology, wildcat wells, Tertiary plant fossil localities, K-Ar
559 age dates, and petroleum operations, Cook Inlet area, Alaska, *U.S. Geol. Survey Miscellaneous Investigation Series I-1019*
560 (1976).
- 561 [34] G. Plafker, L. M. Gilpin, J. C. Lahr, Neotectonic Map of Alaska, in: G. Plafker, H. C. Berg (Eds.), *Geology of Alaska,*
562 Vol. G-1 of *The Geology of North America*, Geol. Soc. Am., Boulder, Colo., USA, 1994, Plate 12.
- 563 [35] P. J. Haeussler, R. L. Bruhn, T. L. Pratt, Potential seismic hazards and tectonics of the upper Cook Inlet basin, Alaska,
564 based on analysis of Pliocene and younger deformation, *Geol. Soc. Am. Bull.*112 (9) (2000) 1414–1429.
- 565 [36] R. L. Bruhn, P. J. Haeussler, Deformation driven by subduction and microplate collision: Geodynamics of Cook Inlet
566 basin, *Geol. Soc. Am. Bull.*118 (3/4) (2006) 289–303.
- 567 [37] K. A. Lewis, C. J. Potter, A. K. Shah, R. G. Stanley, P. J. Haeussler, R. W. Saltus, Preliminary Interpretation of Industry
568 Two-Dimensional Seismic Data from Susitna Basin, South-Central Alaska, *U.S. Geol. Survey open-file report* 2015-1138
569 (2015). doi:10.3133/ofr20151138.
- 570 [38] A. K. Shah, R. G. Stanley, K. Lewis, P. J. Haeussler, C. J. Potter, R. W. Saltus, J. D. Phillips, Aeromagnetic survey
571 data used to map features of the Cook Inlet and Susitna basins, Alaska, 2015, Abstract presented at 2015 AGU-SEG
572 Workshop, Denver, Colo., 25–27 Aug.
- 573 [39] B. Gutenberg, C. F. Richter, *Seismicity of the Earth and Associated Phenomena*, 2nd Edition, Princeton U. Press,
574 Princeton, New Jersey, USA, 1954.
- 575 [40] F. Waldhauser, W. L. Ellsworth, A double-difference earthquake location algorithm: Method and application to the
576 Northern Hayward fault, California, *Bull. Seismol. Soc. Am.*90 (6) (2000) 1353–1368. doi:10.1785/0120000006.
- 577 [41] D. A. Storchak, D. Di Giacomo, I. Bondár, E. R. Engdahl, J. Harris, W. H. K. Lee, A. Villaseñor, P. Bormann, Public
578 release of the ISC–GEM Global Instrumental Earthquake Catalogue (1900–2009), *Seismol. Res. Lett.*84 (5) (2013) 810–
579 815. doi:10.1785/0220130034.
- 580 [42] International Seismological Centre, ISC-GEM Global Instrumental Earthquake Catalogue, Version 5.0, released on 2018-
581 02-27 (2018).
- 582 [43] E. R. Engdahl, R. van der Hilst, R. Buland, Global teleseismic earthquake relocation with improved travel times and
583 procedures for depth determination, *Bull. Seismol. Soc. Am.*88 (3) (1998) 722–743.
- 584 [44] I. Bondár, D. Storchak, Improved location procedures at the International Seismological Centre, *Geophys. J. Int.*186
585 (2011) 1220–1244. doi:10.1111/j.1365-246X.2011.05107.x.
- 586 [45] D. D. Giacomo, I. Bondár, D. A. Storchak, E. R. Engdahl, P. Bormann, J. Harris, ISC-GEM: Global instrumental earth-
587 quake catalogue (1900–2009), III. re-computed MS and mb, proxy MW, final magnitude composition and completeness
588 assessment, *Physics of the Earth and Planetary Interiors* 239 (2015) 33–47. doi:10.1016/j.pepi.2014.06.005.
- 589 [46] C. Flores, D. I. Doser, Shallow seismicity of the Anchorage, Alaska, Region (1964–1999), *Bull. Seismol. Soc. Am.*95 (5)
590 (2005) 1865–1879. doi:10.1785/0120040121.
- 591 [47] D. I. Doser, Historical seismicity (1918–1964) of the Kodiak Island region, *Bull. Seismol. Soc. Am.*95 (3) (2005) 878–895.
592 doi:10.1785/0120040175.
- 593 [48] D. I. Doser, Relocations of earthquakes (1899–1917) in south-central Alaska, *Pure App. Geophys.*163 (2006) 1461–1476.
594 doi:10.1007/s00024-006-0085-3.

- 595 [49] A. Lomax, J. Virieux, P. Volant, C. Berge, Probabilistic earthquake location in 3D and layered models: Introduction of
 596 a Metropolis-Gibbs method and comparison with linear locations, in: C. H. Thurber, N. Rabinowitz (Eds.), *Advances in*
 597 *Seismic Event Location*, Kluwer, Amsterdam, 2000, pp. 101–134.
- 598 [50] B. L. N. Kennett, E. R. Engdahl, R. Buland, Constraints on seismic velocities in the Earth from traveltimes, *Geophys. J. Int.* 122 (1995) 108–124.
- 600 [51] H. P. Crotwell, T. J. Owens, J. Ritsema, The TauP Toolkit: Flexible Seismic travel-time and ray-path utilities, *Seismol. Res. Lett.* 70 (2) (1999) 154–160.
- 602 [52] International Seismological Centre, On-line Bulletin, <http://www.isc.ac.uk>, Internat'l. Seis. Cent., Thatcham, United Kingdom (accessed 2017-05-03) (2015).
- 604 [53] A. Lomax, V. Silwal, C. Tape, Hypocenter estimation for 14 earthquakes in south-central Alaska (1929–1975), ScholarWorks@UA at <http://hdl.handle.net/11122/8380>: descriptor file and zipped set of text files for each earthquake (2018).
- 606 [54] H. O. Wood, F. Neumann, Modified Mercalli intensity scale of 1931, *Bull. Seismol. Soc. Am.* 21 (4) (1931) 277–283.
- 608 [55] S. R. Brockman, A. F. Espinosa, J. A. Michael, Catalog of Intensities and Magnitudes for Earthquakes in Alaska and
 609 the Aleutian Islands—1786–1981, 1988, U.S. Geol. Survey Bulletin 1840.
- 610 [56] A. Tarantola, *Inverse Problem Theory and Methods for Model Parameter Estimation*, SIAM, Philadelphia, Penn., USA,
 611 2005.
- 612 [57] G. Abers, D. Christensen, Seismic and geodetic imaging of subducting terranes under North America, *International*
 613 *Federation of Digital Seismograph Networks. Other/Seismic Network.* doi:10.7914/SN/YV_2006 (2006).
- 614 [58] C. Tape, D. Christensen, M. M. Moore-Driskell, J. Sweet, K. Smith, Southern Alaska Lithosphere and Mantle Observ-
 615 *ation Network (SALMON): a seismic experiment covering the active arc by road, boat, plane, and helicopter, Seismol. Res. Lett.* 88 (4) (2017) 1185–1202. doi:10.1785/0220160229.
- 617 [59] C. Tape, D. H. Christensen, M. M. Driskell, Southern Alaska Lithosphere and Mantle Observation Network, *International*
 618 *Federation of Digital Seismograph Networks. Other/Seismic Network.* doi:10.7914/SN/ZE_2015 (2015).
- 619 [60] V. Silwal, C. Tape, Seismic moment tensors and estimated uncertainties in southern Alaska, *J. Geophys. Res. Solid*
 620 *Earth* 121 (2016) 2772–2797. doi:10.1002/2015JB012588.
- 621 [61] L.-S. Zhao, D. V. Helmberger, Source estimation from broadband regional seismograms, *Bull. Seismol. Soc. Am.* 84 (1)
 622 (1994) 91–104.
- 623 [62] L. Zhu, D. Helmberger, Advancement in source estimation techniques using broadband regional seismograms, *Bull. Seismol. Soc. Am.* 86 (5) (1996) 1634–1641.
- 625 [63] L. Zhu, L. A. Rivera, A note on the dynamic and static displacements from a point source in multilayered media, *Geophys. J. Int.* 148 (2002) 619–627. doi:10.1046/j.1365-246X.2002.01610.x.
- 627 [64] C. Alvizuri, C. Tape, Full moment tensors for small events ($M_w < 3$) at Uturuncu volcano, Bolivia, *Geophys. J. Int.* 206
 628 (2016) 1761–1783. doi:10.1093/gji/ggw247.
- 629 [65] C. Alvizuri, V. Silwal, L. Krischer, C. Tape, Estimation of full moment tensors, including uncertainties, for nuclear explo-
 630 *sions, volcanic events, and earthquakes, J. Geophys. Res. Solid Earth* 123 (2018) 5099–5119. doi:10.1029/2017JB015325.
- 631 [66] S. R. Ford, W. R. Walter, D. S. Dreger, Event discrimination using regional moment tensors with teleseismic-*P* constraints, *Bull. Seismol. Soc. Am.* 102 (2) (2012) 867–872. doi:10.1785/0120110227.
- 633 [67] A. Guilhem, L. Hutchings, D. S. Dreger, L. R. Johnson, Moment tensor inversions of $M \sim 3$ earthquakes in the Geysers
 634 *geothermal fields, California, J. Geophys. Res. Solid Earth* 119 (3) (2014) 2121–2137. doi:10.1002/2013JB010271.
- 635 [68] A. Chiang, D. S. Dreger, S. R. Ford, W. R. Walter, Source characterization of underground explosions from
 636 combined regional moment tensor and first-motion analysis, *Bull. Seismol. Soc. Am.* 104 (4) (2014) 1587–1600.
 637 doi:10.1785/0120130228.

- 638 [69] Z. Wéber, Probabilistic joint inversion of waveforms and polarity data for double-couple focal mechanisms of local
639 earthquakes, *Geophys. J. Int.* 213 (2018) 1586–1598. doi:10.1093/gji/ggy096.
- 640 [70] S. C. Stähler, K. Sigloch, Fully probabilistic seismic source inversion – Part 2: Modelling errors and station covariances,
641 *Solid Earth* 7 (2016) 1521–1536. doi:10.5194/se-2016-87.
- 642 [71] M. Mustać, H. Tkalcic, Point source moment tensor inversion through a Bayesian hierarchical model, *Geophys. J. Int.* 204
643 (2016) 311–323. doi:10.1093/gji/ggv458.
- 644 [72] M. Mustać, H. Tkalcic, On the use of data noise as a site-specific weight parameter in a hierarchical Bayesian moment
645 tensor inversion: The case study of The Geysers and Long Valley caldera earthquakes, *Bull. Seismol. Soc. Am.* 107 (4)
646 (2017) 1914–1922. doi:10.1785/0120160379.
- 647 [73] C. Alvizuri, C. Tape, Full moment tensor analysis of nuclear explosions in North Korea, *Seismol. Res. Lett.* (in press).
- 648 [74] V. Silwal, Seismic moment tensor catalog for crustal earthquakes in the Cook Inlet and Susitna region of southern Alaska,
649 ScholarWorks@UA at <http://hdl.handle.net/11122/8383>: descriptor file, text file of catalog, figures with waveform fits,
650 and input weight files (2018).
- 651 [75] P. Reasenberg, D. Oppenheimer, FPFIT, FPPILOT and FPPAGE: Fortran computer programs for calculating and dis-
652 playing earthquake fault-plane solutions, Open-File Report 85-739 (1985).
- 653 [76] E. Hauksson, P. Shearer, Southern California hypocenter relocation with waveform cross-correlation, Part 1: Results
654 using the double-difference method, *Bull. Seismol. Soc. Am.* 95 (3) (2005) 896–903.
- 655 [77] P. Shearer, E. Hauksson, G. Lin, Southern California hypocenter relocation with waveform cross-correlation, Part
656 2: Results using source-specific station terms and cluster analysis, *Bull. Seismol. Soc. Am.* 95 (3) (2005) 904–915.
657 doi:10.1785/0120040168.
- 658 [78] H. Zhang, C. H. Thurber, Double-difference tomography: the method and its application to the Hayward fault, California,
659 *Bull. Seismol. Soc. Am.* 93 (5) (2003) 1875–1889. doi:10.1785/0120020190.
- 660 [79] N. A. Ratchkovsky, J. Pujol, N. N. Biswas, Relocation of shallow earthquakes in southern Alaska using Joint Hypocenter
661 Determination method, *J. Seis.2* (1998) 87–102.
- 662 [80] A. Douglas, Joint epicentre determination, *Nature* 215 (1967) 47–48.
- 663 [81] R. W. Saltus, R. G. Stanley, P. J. Haeussler, J. V. Jones III, C. J. Potter, K. A. Lewis, Late Oligocene to present
664 contractional structure in and around the Susitna basin, Alaska—Geophysical evidence and geological implications,
665 *Geosphere* 12 (5) (2016) 1–13. doi:10.1130/GES01279.1.
- 666 [82] K. D. Ridgway, J. M. Trop, E. S. Finzel, Modification of continental forearc basins by flat-slab subduction processes: A
667 case study from southern Alaska, in: C. Busby, A. A. Perez (Eds.), *Tectonics of Sedimentary Basins: Recent Advances*,
668 Wiley-Blackwell, 2012, pp. 327–346. doi:10.1002/9781444347166.ch16.
- 669 [83] D. L. LePain, R. G. Stanley, N. T. Harun, K. P. Helmold, R. M. Tsigonis, Reconnaissance stratigraphic studies in the
670 Susitna basin, Alaska, during the 2014 field season, Preliminary Interpretive Report 2015-3-2 (2015). doi:10.14509/29466.
- 671 [84] S. W. Hackett, Gravity survey of Beluga Basin and adjacent area, Cook Inlet region, southcentral Alaska (1977).
672 doi:10.14509/377.
- 673 [85] R. J. Gillis, T. M. Herriott, R. M. Tsigonis, Preliminary results of reconnaissance structural studies of the western Susitna
674 basin, south-central Alaska, Preliminary Interpretive Report 2015-3-5 (2015). doi:10.14509/29469.
- 675 [86] M. A. Fisher, L. B. Magoon, Geologic framework of lower Cook Inlet, *Am. Assoc. Petroleum Geol. Bull.* 62 (3) (1978)
676 373–402.
- 677 [87] D. P. Shellenbaum, L. S. Gregersen, P. R. Delaney, Top Mesozoic unconformity depth map of the Cook Inlet Basin,
678 Alaska, Alaska Div. Geol. Geophys. Surv. Report of Investigation 2010-2, 1 sheet, scale 1:500,000, available at <http://www.dggs.alaska.gov/pubs/id/21961> (last accessed 2016-10-30) (2010). doi:10.14509/21961.
- 679 [88] D. L. LePain, R. G. Stanley, K. P. Helmold, D. P. Shellenbaum, Geologic Framework and Petroleum Sys-

- tems of Cook Inlet Basin, South-Central Alaska, Vol. 104, American Association of Petroleum Geologists, 2013.
doi:10.1306/13491874M1043621.
- [89] J. T. Freymueller, H. Woodard, S. C. Cohen, R. Cross, J. Elliott, C. F. Larsen, S. Hreinsdóttir, C. Zweck, Active deformation processes in Alaska, based on 15 years of GPS measurements, in: J. T. Freymueller, P. J. Haeussler, R. Wesson, G. Ekström (Eds.), *Active Tectonics and Seismic Potential of Alaska*, Vol. 179 of *Geophysical Monograph*, Am. Geophys. Un., Washington, D.C., 2008, pp. 1–42.
- [90] P. O. Koons, B. P. Hooks, T. Pavlis, P. Upton, A. D. Barker, Threedimensional mechanics of Yakutat convergence in the southern Alaskan plate corner, *Tectonics*29. doi:10.1029/2009TC002463.
- [91] M. A. Jadamec, M. I. Billen, S. M. Roeske, Three-dimensional numerical models of flat slab subduction and the Denali fault driving deformation in south-central Alaska, *Earth Planet. Sci. Lett.*376 (2013) 29–42.
- [92] F. H. Wilson, C. P. Hults, H. R. Schmoll, P. J. Haeussler, J. M. Schmidt, L. A. Yehle, K. A. Labay, Preliminary Geologic Map of the Cook Inlet Region, Alaska, Open-File Report 2009-1108 (2009).
- [93] P. J. Haeussler, A. Matmon, D. P. Schwartz, G. G. Seitz, Neotectonics of interior Alaska and the late Quaternary slip rate along the Denali fault system, *Geosphere*13 (5) (2017) 1445–1463. doi:10.1130/GES01447.1.
- [94] P. M. Shearer, G. A. Prieto, E. Hauksson, Comprehensive analysis of earthquake source spectra in southern California, *J. Geophys. Res.*111. doi:10.1029/2005JB003979.
- [95] P. M. Mai, G. C. Beroza, Source scaling properties from finite-fault-rupture models, *Bull. Seismol. Soc. Am.*90 (3) (2000) 604–615.
- [96] Z. Duputel, L. Rivera, H. Kanamori, G. Hayes, W phase source inversion for moderate to large earthquakes, *Geophys. J. Int.*189 (2012) 1125–1147.
- [97] K. Abe, Magnitudes of large shallow earthquakes from 1904 to 1980, *Phys. Earth Planet. Inter.*27 (1981) 72–92.
- [98] E. R. Engdahl, A. Villaseñor, Global seismicity: 1900–1999, in: W. H. K. Lee, H. Kanamori, P. C. Jennings, C. Kisslinger (Eds.), *International Handbook of Earthquake and Engineering Seismology*, Vol. 81A of *International Geophysics Series*, Academic Press, London, 2002, pp. 665–690.
- [99] M. A. Jadamec, M. I. Billen, Reconciling surface plate motions with rapid three-dimensional mantle flow around a slab edge, *Nature*465 (2010) 338–342. doi:10.1038/nature09053.
- [100] G. P. Hayes, D. J. Wald, R. L. Johnson, Slab1.0: A three-dimensional model of global subduction zone geometries, *J. Geophys. Res.*117. doi:10.1029/2011JB008524.
- [101] Y. Wang, C. Tape, Seismic velocity structure and anisotropy of the Alaska subduction zone derived from surface wave tomography, *J. Geophys. Res. Solid Earth*119 (2014) 8845–8865. doi:10.1002/2014JB011438.
- [102] C. Amante, B. W. Eakins, ETOPO1 1 Arc-Minute Global Relief Model: Procedures, Data Sources and Analysis, NOAA Technical Memorandum NESDIS NGDC-24, 19 pp. (2009).
- [103] R. G. Stanley, P. J. Haeussler, J. A. Benowitz, D. K. Goodman, R. L. Ravn, D. P. Shellenbaum, R. W. Saltus, K. A. Lewis, C. J. Potter, New stratigraphic revelations in the subsurface Susitna basin, south-central Alaska, from geochronology and biostratigraphy [poster]: GSA Cordilleran Section Meeting, Fresno, CA, May 22, 2013: Alaska Division of Geological & Geophysical Surveys, 1 sheet. <http://doi.org/10.14509/26887> (2013).
- [104] J. G. Meyer Jr., Principal facts for gravity data collected in the northern Susitna Basin area, southcentral Alaska, Alaska Div. Geol. Geophys. Surv. Preliminary Interpretive Report 2005-5 (2005).
- [105] A. J. Wickens, J. H. Hodgson, Computer Re-Evaluation of Earthquake Mechanism Solutions, Publications of the Dominion Observatory, Vol. 33, No. 1, Ottawa, Canada Department of Energy, Mines, and Resources, Contribution 103 to the International Upper Mantle Project (1967).
- [106] F. Neumann, United States Earthquakes 1933, U.S. Department of Commerce, 1935.
- [107] R. R. Bodle, United States Earthquakes 1943, U.S. Department of Commerce, 1945.

⁷²⁴ [108] L. M. Murphy, W. K. Cloud, United States Earthquakes 1954, U.S. Department of Commerce, 1956.

Table 1: Earthquake selection for three target subregions and for the full region. N_e is the number of earthquakes analyzed in each region for a particular method.

Region	longitude		latitude		method	N_e	max depth (km)	min mag	date range
	min (°)	max (°)	min (°)	max (°)					
Beluga region	-151.50	-151.10	61.25	61.90	moment tensor	9	30	M_l 2.5	2007-08-15 2017-01-01
upper Cook Inlet region	-151.50	-150.60	60.60	61.25	moment tensor	22	30	M_l 2.5	2007-08-15 2017-01-01
Susitna region	-151.10	-149.90	61.50	62.50	moment tensor	22	30	M_l 3.0	2007-08-15 2017-01-01
Cook Inlet and Susitna region	-151.75	-149.50	60.50	62.50	historical	12	200	M_w 5.8	1904-01-01 2017-01-01
	-152.00	-149.00	60.50	62.50	double difference	5726	30	M_l 1.5	1990-01-01 2017-01-01

Table 2: Earthquakes $M \geq 5.8$ in the Cook Inlet and Susitna region (Table 1) of south-central Alaska since the start of the instrumental era in 1904. The events are selected from the ISC-GEM catalog (before 1976-01-01) and GCMT catalog (after 1976-01-01). Depth estimates are listed in Table 3. ISCG = ISC-GEM 5.0 [41], GCMT = Global Centroid Moment Tensor catalog [28, 29]. NA means that the earthquake was outside the time interval of a particular study.

origin time	longitude	latitude	ref.	mag.	ref.	GR	Abe	EV	DB
						[39]	[97]	[98]	[32]
				M_w		M	M_s, m_b	M_w	M_w
1933-04-27 02:36:07	-151.06	61.10	ISCG	6.78	ISCG	7.0	6.9, 7.1	6.90	7.0
1933-06-12 15:23:41	-151.35	61.23	ISCG	5.82	ISCG	—	—	—	—
1933-06-13 22:19:51	-151.67	61.22	ISCG	5.97	ISCG	6.25	—	—	—
1933-06-19 18:47:46	-151.03	61.39	ISCG	5.85	ISCG	6.0	—	—	—
1934-06-18 09:13:52	-151.40	60.72	ISCG	5.97	ISCG	6.75	—	6.60	6.1
1936-10-23 06:24:21	-151.01	61.17	ISCG	6.82	ISCG	—	—	—	—
1941-07-30 01:51:29	-150.97	60.90	ISCG	6.39	ISCG	6.25	—	—	6.3
1943-11-03 14:32:20	-151.00	61.79	ISCG	7.34	ISCG	7.3	7.4, 7.1	7.20	7.0
1954-10-03 11:18:48	-150.39	60.65	ISCG	6.36	ISCG	NA	—	—	6.6
1974-12-29 18:25:01	-150.58	61.59	ISCG	5.92	ISCG	NA	—	—	NA
1975-01-01 03:55:13	-149.82	61.90	ISCG	5.92	ISCG	NA	—	7.40	NA
1991-05-01 07:18:46	-151.42	62.47	GCMT	6.30	GCMT	NA	NA	6.2	NA

Table 3: Estimated depths, with uncertainties, for the earthquakes in Table 2. Depths are listed in km below sea level. The depths from NonLinLoc (NLL) are for the maximum likelihood, and the uncertainty value is \sqrt{covZZ} , where $covZZ$ can be found in the NLL output files in [53]. See also Figure 7 for examples of depth distributions of all posterior hypocenters. The right three columns list the vertical distance from the ISC-GEM epicenter to the subduction interface, for three different interface models. Events marked as * are likely slab events. For the Engdahl catalog, DEQ means that depth is a free parameter, and FEQ means that depth is fixed based on independent information.

	NLL (this study)	GR [39]	DB [32]	EV [98]	ISCG [41]	JB10 [99]	H12 [100]	L13 [10]
1933-04-27	0.33 ± 5	0	9 ± 4	35 (FEQ)	15 ± 4	54	68	63
1933-06-12	0.65 ± 20	0	—	—	15 ± 9	71	77	73
1933-06-13	12.71 ± 4	0	—	—	15 ± 9	85	87	82
1933-06-19	16.29 ± 6	0	—	—	15 ± 7	64	71	66
1934-06-18*	49.20 ± 4	80	76 ± 10	50 (DEQ)	60 ± 9	63	72	66
1936-10-23	0.33 ± 4	—	—	—	15 ± 14	56	68	63
1941-07-30	0.33 ± 6	0	—	—	35 ± 14	49	64	59
1943-11-03	17.27 ± 3	0	27 ± 4	35 (FEQ)	15 ± 4	73	75	71
1954-10-03*	55.88 ± 2	N/A	60 ± 10	64	62 ± 5	40	52	45
1974-12-29*	68.10 ± 4	N/A	N/A	—	65 ± 5	56	64	57
1975-01-01*	64.03 ± 3	N/A	N/A	—	63 ± 5	43	57	48
		GCMT	AEC					
1991-05-01*		118	115	114 (DEQ)	113 ± 5	123	110	100

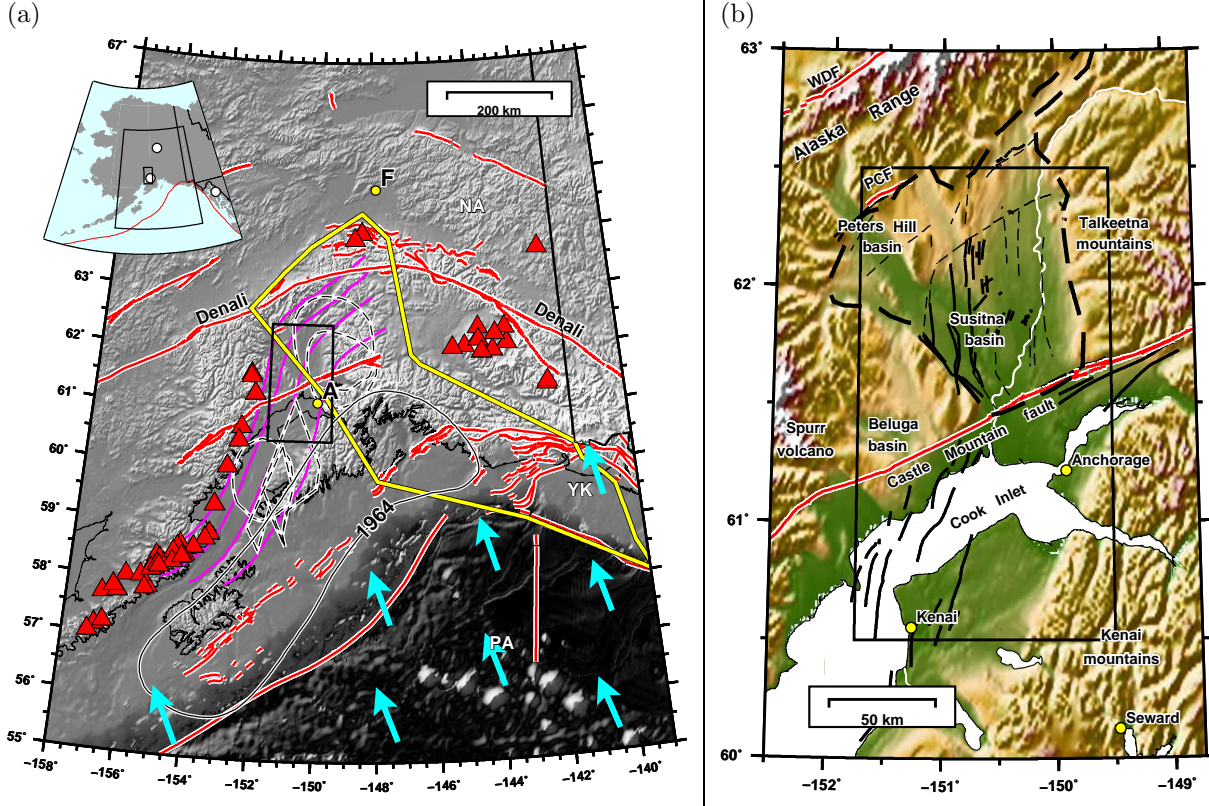


Figure 1: (a) Active tectonic setting of the Aleutian–Alaskan subduction zone, south-central Alaska. The rectangle in the middle shows the main study region. Cyan arrows shows the plate vectors for the subducting Pacific plate (PA) under the North American plate (NA) [2]. Red lines denote active faults [19]. Magenta curves are the 40 km, 60 km, 80 km, and 100 km contours of the subduction interface, i.e.,, the top of the Pacific plate [10]. Yellow bounded region denotes the surface and subsurface extent of the Yakutat block (YK) [4]. Red triangles represent active volcanoes. Black dashed lines are inferred slow slip events from various sources [14, 15, 16, 17]. Also marked is the aftershock zone of the 1964 M_w 9.2 earthquake. Labeled cities: Anchorage (A) and Fairbanks (F). (b) Physiographic map of the Cook Inlet and Susitna region, south-central Alaska. Active faults are plotted in red and include Castle Mountain, Pass Creek (PCF), and the western Denali fault (WDF) at upper left [19]. Cook Inlet sedimentary basin underlies Cook Inlet and the western Kenai peninsula [87] (Figure 3). North of the Castle Mountain fault are three sedimentary basins: Beluga, Susitna, and Peters Hill. Active folds in Cook Inlet basin [19] are marked in black. Other faults in Susitna basin also marked in black are obtained from [8, 38] (Figure S1). The thick black dashed line denotes the boundary of Susitna lowlands [9].

725 Figure 2 [FOLLOWING PAGE]:
726 Seismicity in south-central Alaska. (a) Alaska Earthquake Center (AEC) catalog: $M_w \geq 2$, 1990-01-01 to
727 2017-01-01, colored by depth. The box, containing Anchorage (A), is the focus region of this study; the
728 two profiles are shown in (b) and (c). The red lines are the active faults from [19]. The blue line is the
729 lateral extent of slab seismicity, digitized from the full AEC catalog. (b) S–N cross-section of (a) along the
730 longitude line of -150.75° , from latitude 60° to 62.5° . Seismicity within 20 km of the profile is shown. Three
731 large earthquakes of interest are projected onto the profile: 1933 $M_w 6.78$, 1943 $M_w 7.34$, and 1954 $M_w 6.36$;
732 the hypocenters are estimated from NonLinLoc. Geometric boundaries shown are the subduction interface
733 [10], the Moho [101], and topography [102] exaggerated by a factor of 20. (c) SE–NW cross-section of (a)
734 between Anchorage ($x = 0$ km) and the 1943 earthquake.

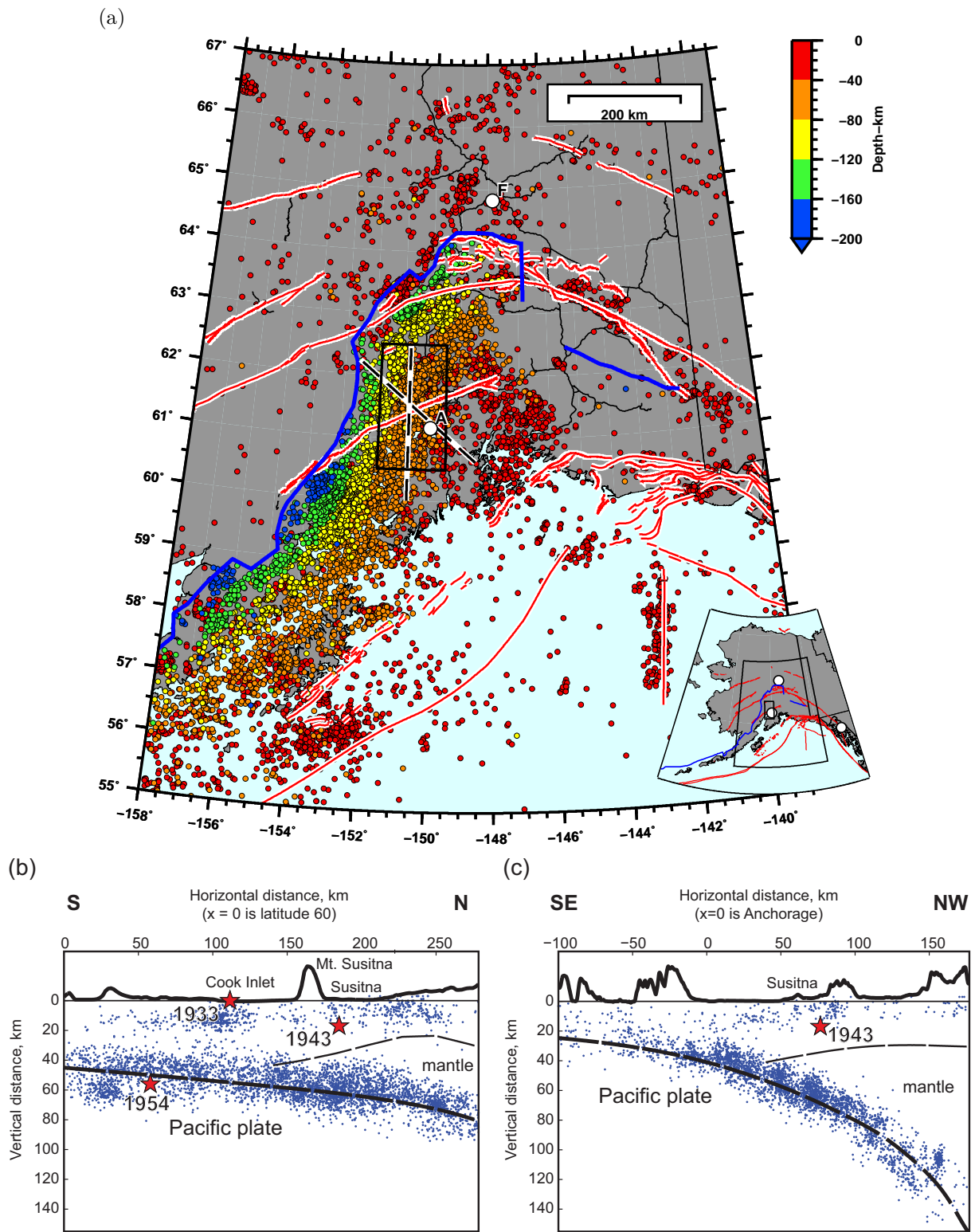


Figure 2:

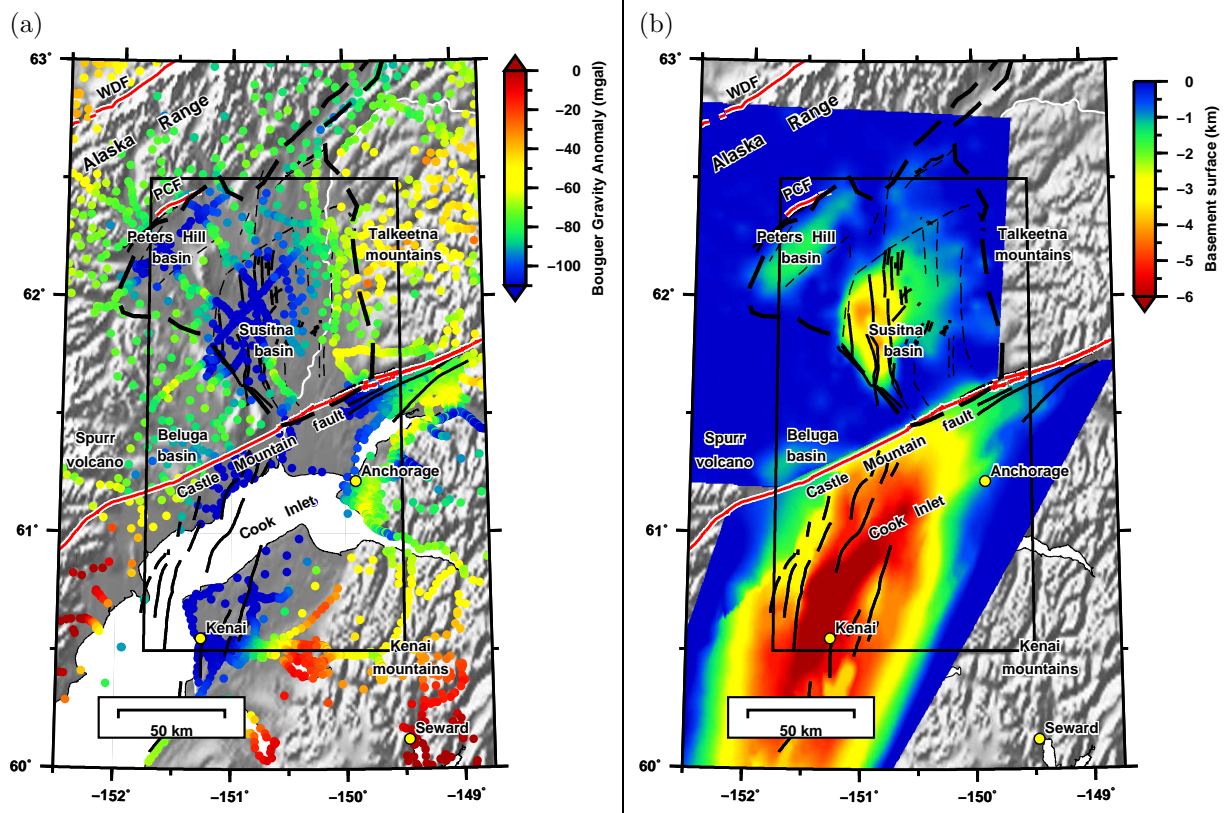


Figure 3: Gravity data and estimated basement depths for the Cook Inlet and Susitna region; see physiographic map in Figure 1b for comparison. Faults and folds plotted include active faults [19], active folds in Cook Inlet [26, 19], and faults in the Susitna basin [37, 8]. (a) Bouguer gravity data [81]. (b) Maps of depth to base of Cenozoic strata in Cook Inlet basin [87], as well as base of Cenozoic strata in Susitna basin [92], Peters Hill basin, and Beluga basin [103]. The dashed outline is the Susitna lowlands region of [9, 104].

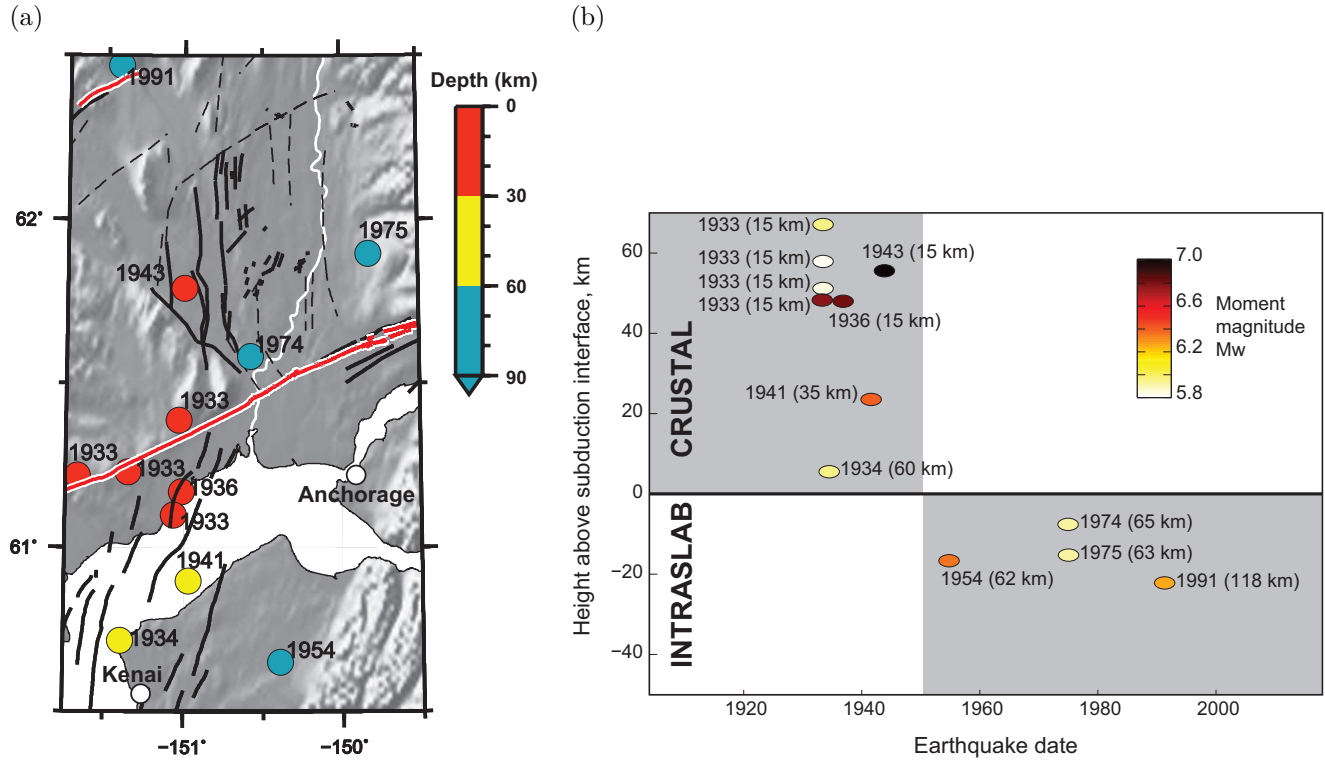


Figure 4: All 12 major earthquakes ($M_w \geq 5.8$) in the Cook Inlet and Susitna region (see Table 1) Earthquakes are selected from the ISC-GEM catalog for the time interval 1904-01-01 to 2017-01-01. (a) Map showing epicenters, colored by depth. (b) Plot of height above subduction interface [10] (Figure 1a) as a function of origin time, for the 12 earthquakes in (a). The checkered shading at the year of 1950 accentuates the pattern of early crustal earthquakes and later (more recent) intraslab earthquakes.

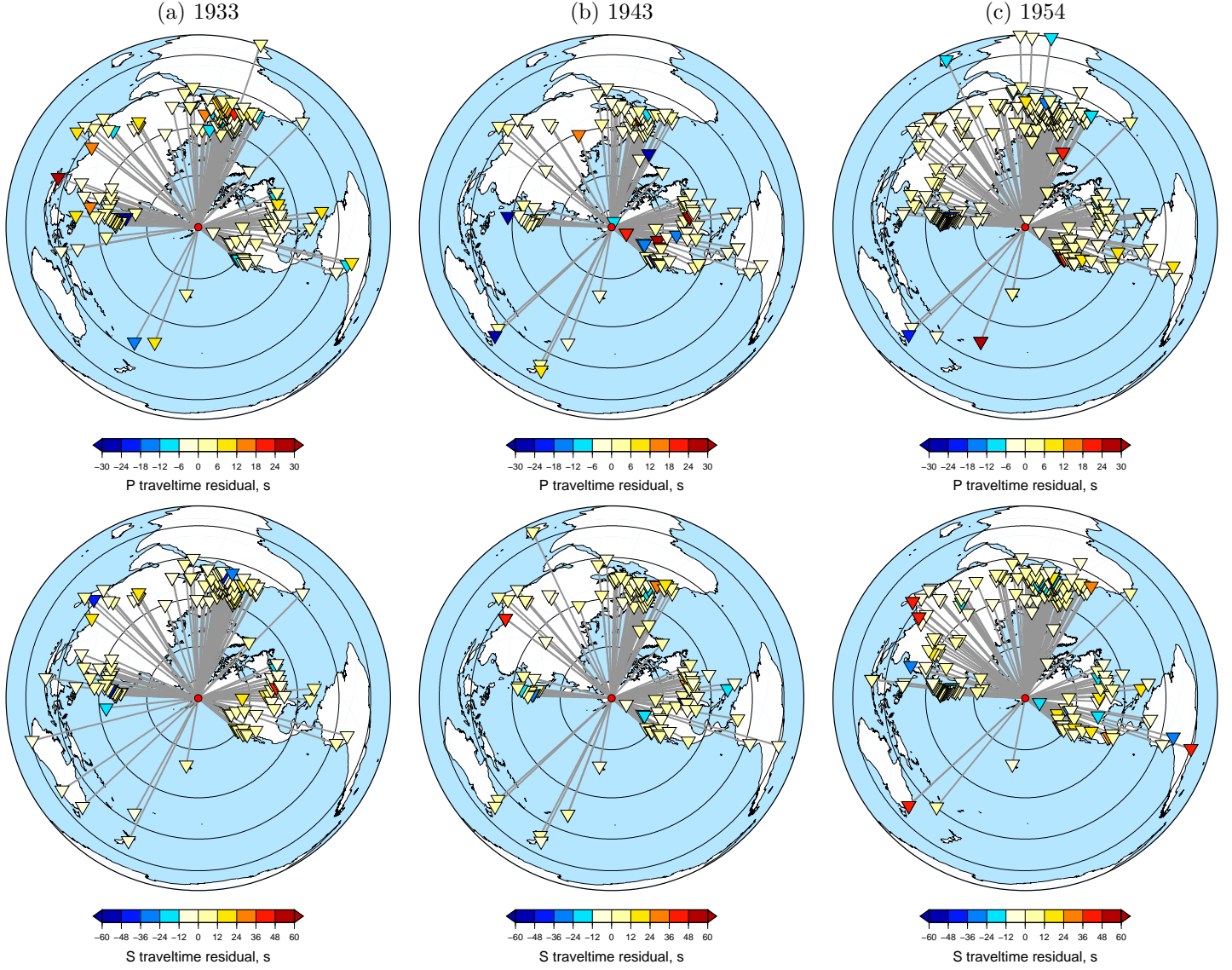


Figure 5: Station coverage for P arrival times (top) and S arrival times (bottom) used in estimating the epicenters for the 1933, 1943, and 1954 Alaska earthquakes. The maximum likelihood epicenter for each earthquake is marked by red circle at the center. The arrival times of the phases were obtained from ISC [52], and the magnitudes listed are from the ISC-GEM catalog (Table 2). The stations are marked by inverted triangles and colored by the difference between the ISC arrival time and synthetic obtained using the `ak135` velocity model [50]. Circles show epicentral distances of $\Delta = 30^\circ, 60^\circ, 90^\circ, 120^\circ$, and 150° . The posterior epicenters for each earthquake are shown in Figure 6. For details of the results, see [53]. (a) 1933 $M_w 6.78$ earthquake. There are 174 P arrival times and 158 S arrival times recorded by 179 stations. (b) 1943 $M_w 7.34$ earthquake. There are 137 P arrival times and 136 S arrival times recorded by 137 stations. (c) 1954 $M_w 6.36$ earthquake. There are 346 P arrival times and 223 S arrival times recorded by 263 stations.

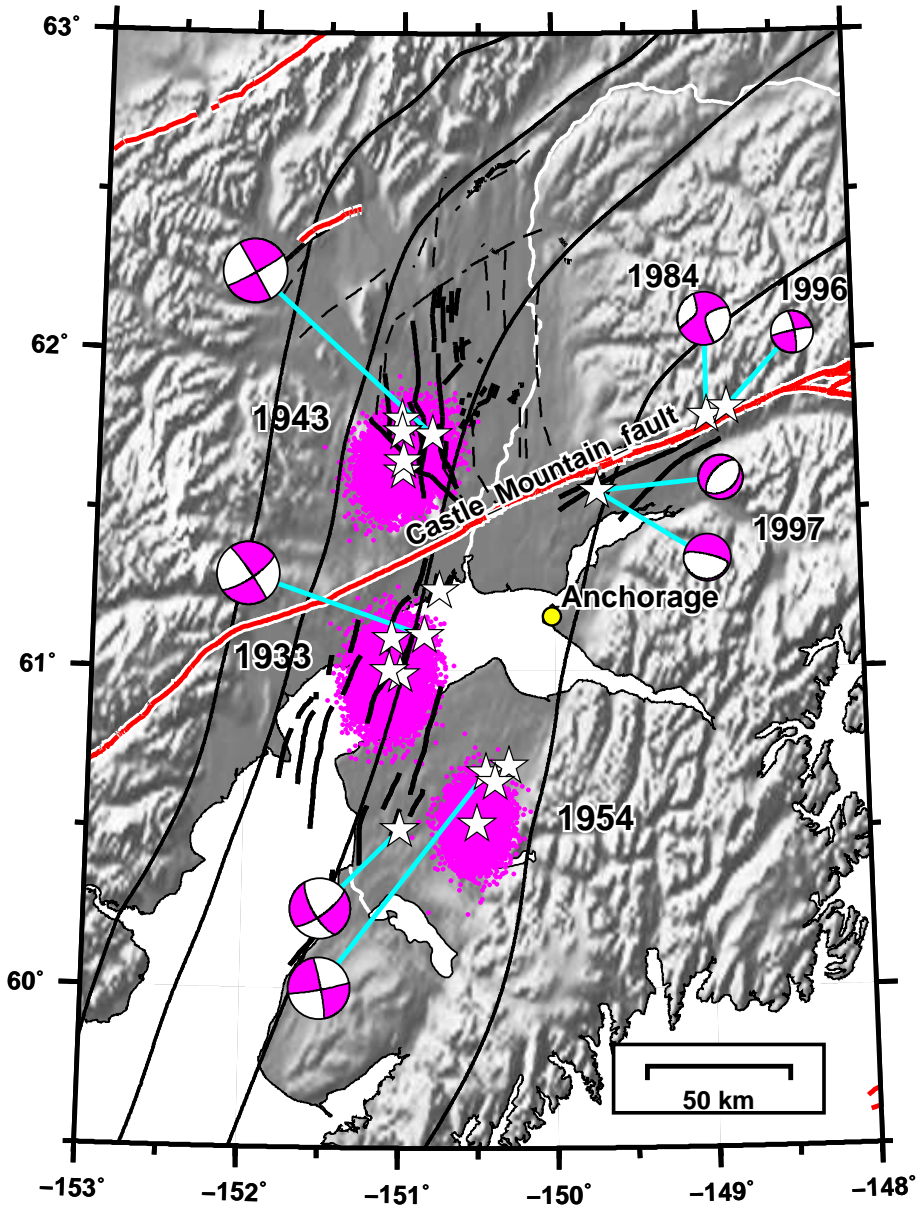


Figure 6: Estimated epicenters for the 1933, 1943, and 1954 earthquakes; see [53] for details. Each cloud of colored dots represents the posterior epicenters, which are centered on a maximum likelihood epicenter (star). Other stars show epicenter estimates from other studies (Table S1: [98, 32, 39, 41]; see also Figure 11). See Figure 7 for information regarding the depths of the posterior samples relative to the underlying subduction interface. Also shown are active faults and folds [19, 8] and contours of the subduction interface (i.e., the top of the subducting Pacific plate) at 40 km, 60 km, 80 km, and 100 km [10]. The beachballs show source mechanisms for 1933 [32], 1943 [32], 1954 [32, 105], 1984 [28], 1996 (AEC), and 1997 (AEC, [28]). The 1984, 1996, and 1997 epicenters are from the AEC catalog.

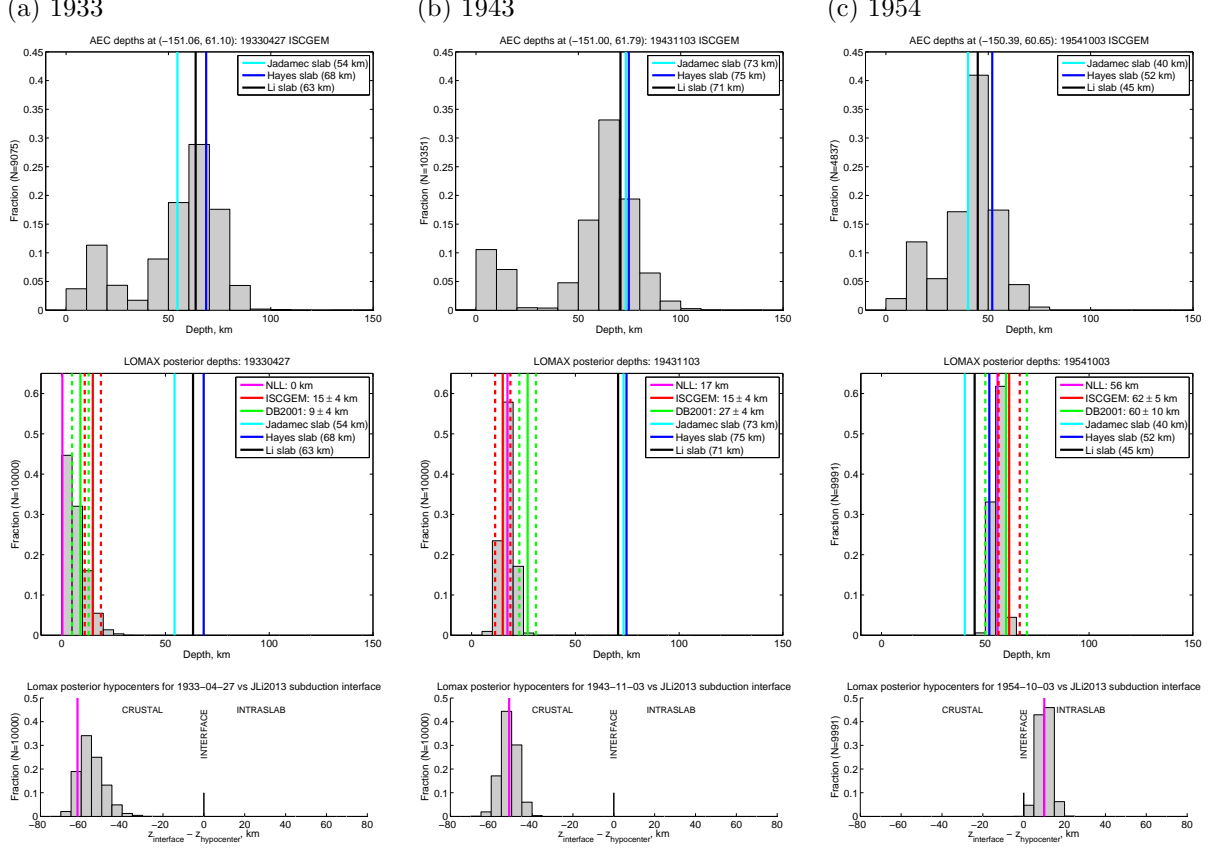


Figure 7: Estimated depth to subduction interface for three historical earthquakes. Each hypocentral estimation using NonLinLoc provides a cloud of posterior hypocenters; see Figure 6 for a map view. For each posterior hypocenter we evaluate the vertical distance to the subduction interface models of [99] (cyan), [100] (blue), and [10] (black). (a) 1933-04-27 M_w 6.8 earthquake. (top) Distribution of depths of modern microseismicity ($M \geq 0$, 2000–2018) whose epicenters are within a 40 km of the ISC-GEM epicenter. (middle) Distribution of depths of posterior hypocenters. Also shown are our maximum-likelihood estimate from NonLinLoc (magenta) and the depth estimates, with uncertainties, from ISC-GEM [41] (red) and DB2001 [32] (green). (bottom) Distribution of vertical distances between our posterior hypocenters and the underlying subduction interface from [10]. Distributions to the left favor a crustal interpretation for the earthquake; distributions to the right favor an intraslab interpretation. (b) 1943-11-03 M_w 7.3 earthquake. (c) 1954-10-03 M_w 6.4 earthquake.

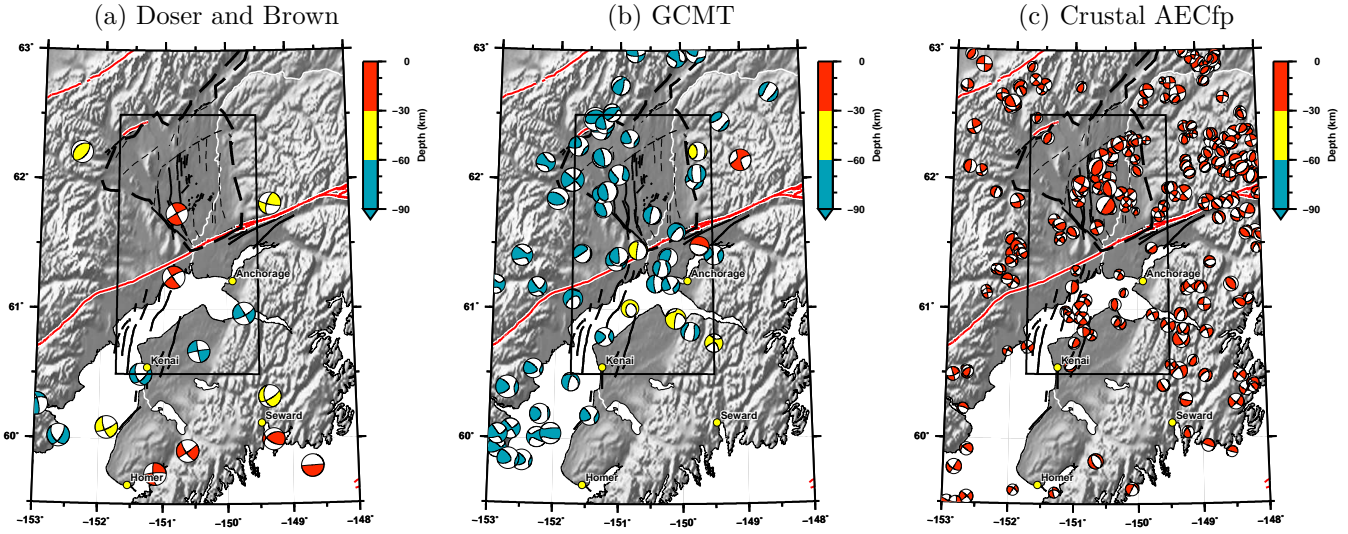


Figure 8: Moment tensor solutions from previous studies. (a) Major historic events (1920–1964), from [32]. The three earthquakes near longitude -150° are, from north to south, the 1943, 1933, and 1954 earthquakes. (b) All events from the GCMT catalog, 1976–2017 [28, 29]. (c) All crustal ($\text{depth} \leq 30 \text{ km}$) events (1990-01-01 to 2017-01-01) from the Alaska Earthquake Center fault-plane catalog. These focal mechanisms are derived from P polarity observations. See Section 2 for more information on major historic events. See Figure 11 for our new moment tensor solutions.

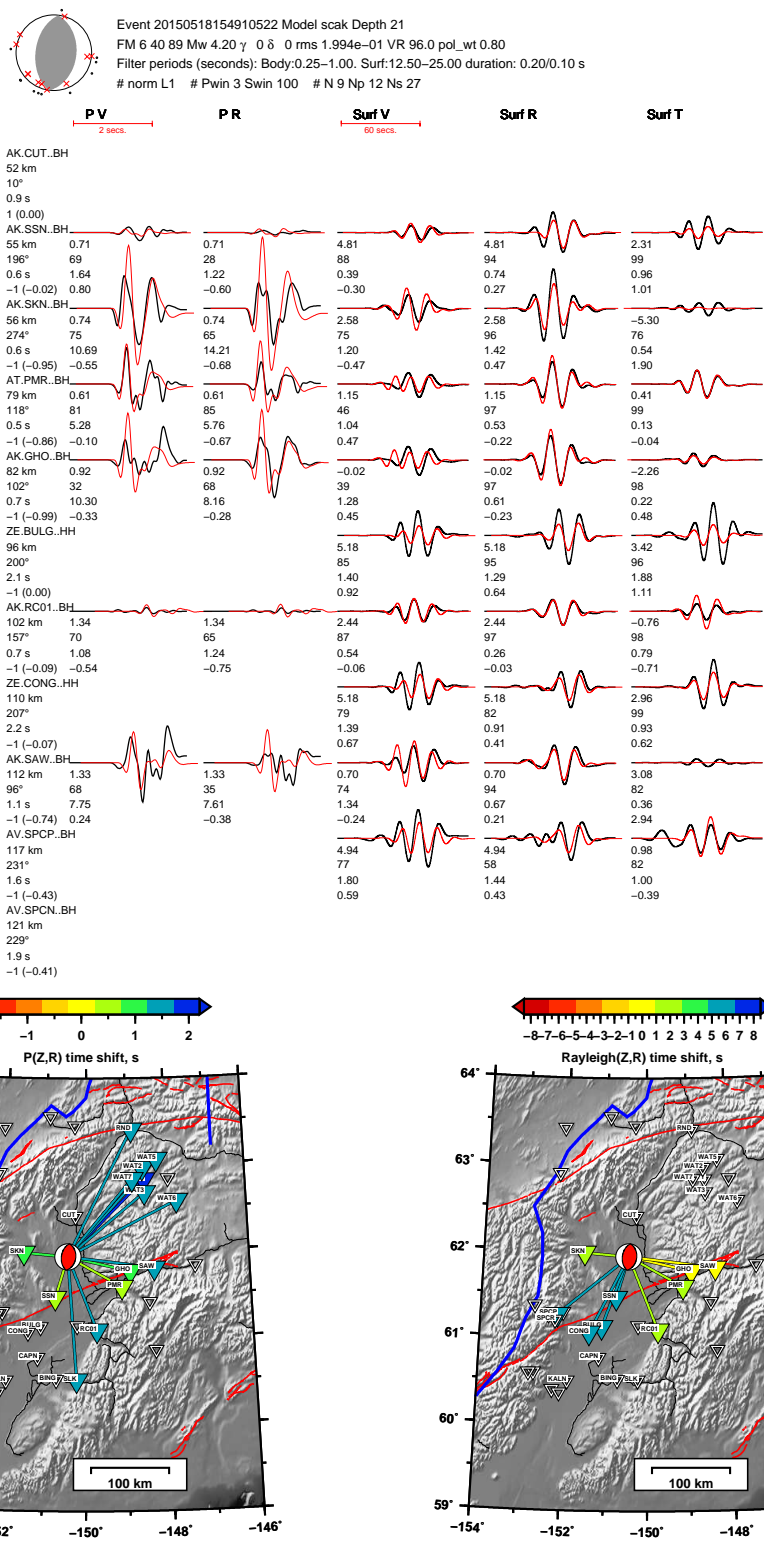


Figure 9: (top) Waveform fits at subset of stations used for a M_w 4.2 crustal earthquake in the Susitna region. See Table S4 for source parameters. Waveform fits for all stations, and for all events, are available [74]. (bottom) Map of time shifts between observed and synthetic waveforms for the P waves (left) and Rayleigh waves (right). Open triangles denote stations with available waveforms that were not used in the inversion. Station names are listed if either the waveform or first-motion polarity was used. Note the large positive time shift for Rayleigh waves traveling to the southwest, through basins. This indicates that along these paths the assumed 1D model is too fast relative to the actual Earth structure.

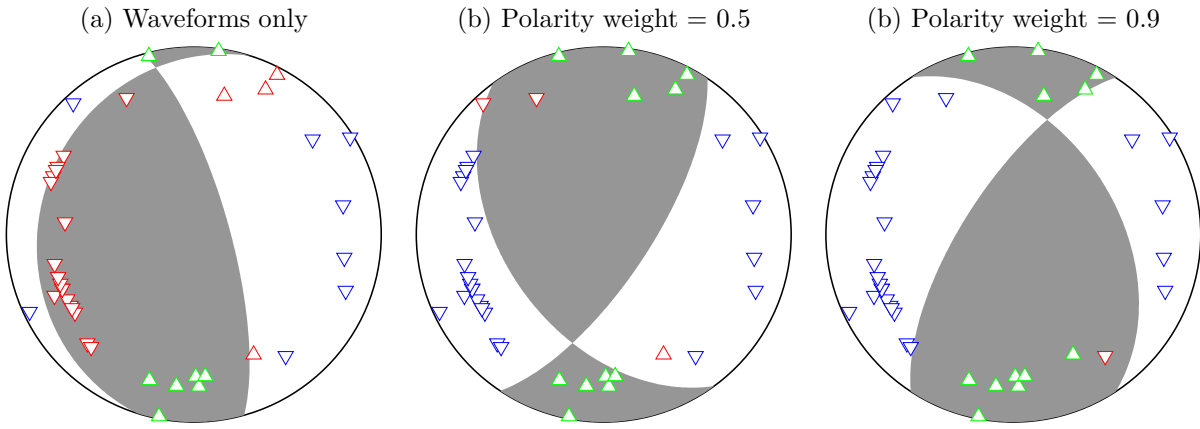


Figure 10: Impact of using different weights for the polarity misfit, shown for an example earthquake in Cook Inlet (eid 20150727022154395). Each beachball shows the best-fitting moment tensor for a given m in Eq. 3. Triangles denote lower-hemisphere piercing points for each ray path from source to station; these are calculated using an assumed 1D Earth model. Upward triangles denote upward polarity observations; downward triangles denote downward polarity observations. The color indicates agreement or not with predicted polarities: red (up or down) indicates mismatch, while green (up) and blue (down) indicate agreement. See Section 3.3 for details on the misfit function. (a) Waveforms only. Note that a large number of polarity mismatches occur. See Figure S6 for waveform fits. (b) Waveforms plus polarities with weight factor 0.5. Here only three polarity measurements are mismatched. See Figure S7 for waveform fits. (c) Waveforms plus polarities with weight factor 0.9. All observed polarities are fit, except one (in red). See Figure S8 for waveform fits.

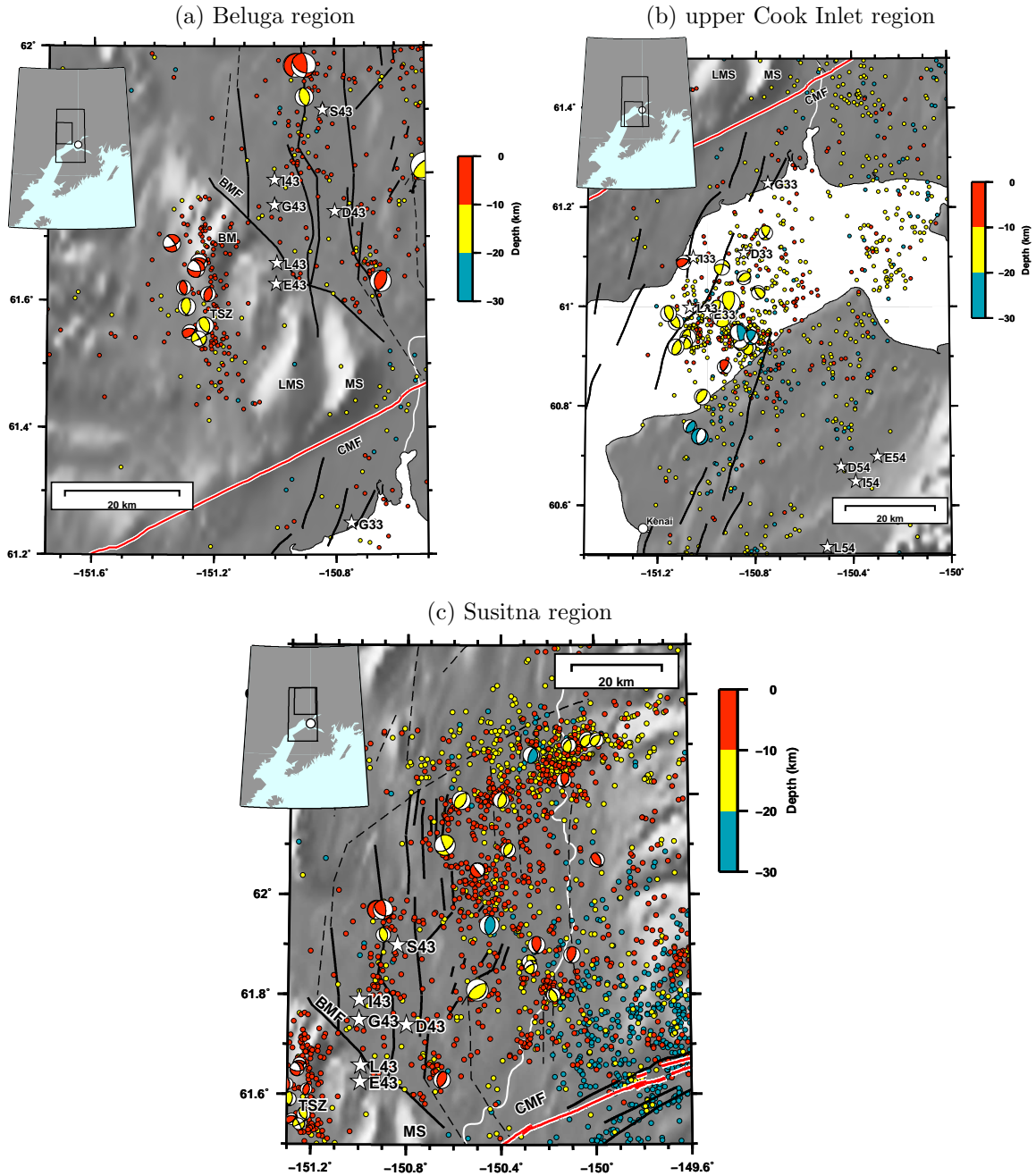


Figure 11: Our double couple moment tensor solutions for crustal earthquakes (depth ≤ 30 km) between 2007-08-15 and 2017-01-01 in three focus regions (Table 1). The displayed regions are slightly larger than the bounding regions listed in Table 1. The color of each moment tensor (beachball) is related to its depth and its size to its magnitude. Also shown are relocated seismicity (Figure 13) and previously published epicenters for the 1933, 1943, and 1954 earthquakes, plotted as stars (Table S1). The maximum likelihood epicenters from this study are labeled as L33, L43, and L54. Text labels: CMF = Castle Mountain fault, BMF = Beluga Mountain fault, BM = Beluga Mountain, LMS = Little Mount Susitna, MS = Mount Susitna, TSZ = Talachulitna seismic zone. Note that the dots here show seismicity, whereas the dots in Figure 6 show our posterior epicenters for the three historical earthquakes. (a) $M_w \geq 2.5$ in the upper Cook Inlet region. (b) $M_w \geq 2.5$ in the Beluga region. (c) $M_w \geq 3.0$ in the Susitna region. See Figure S12 for an alternative version of this figure that includes the basement surface.

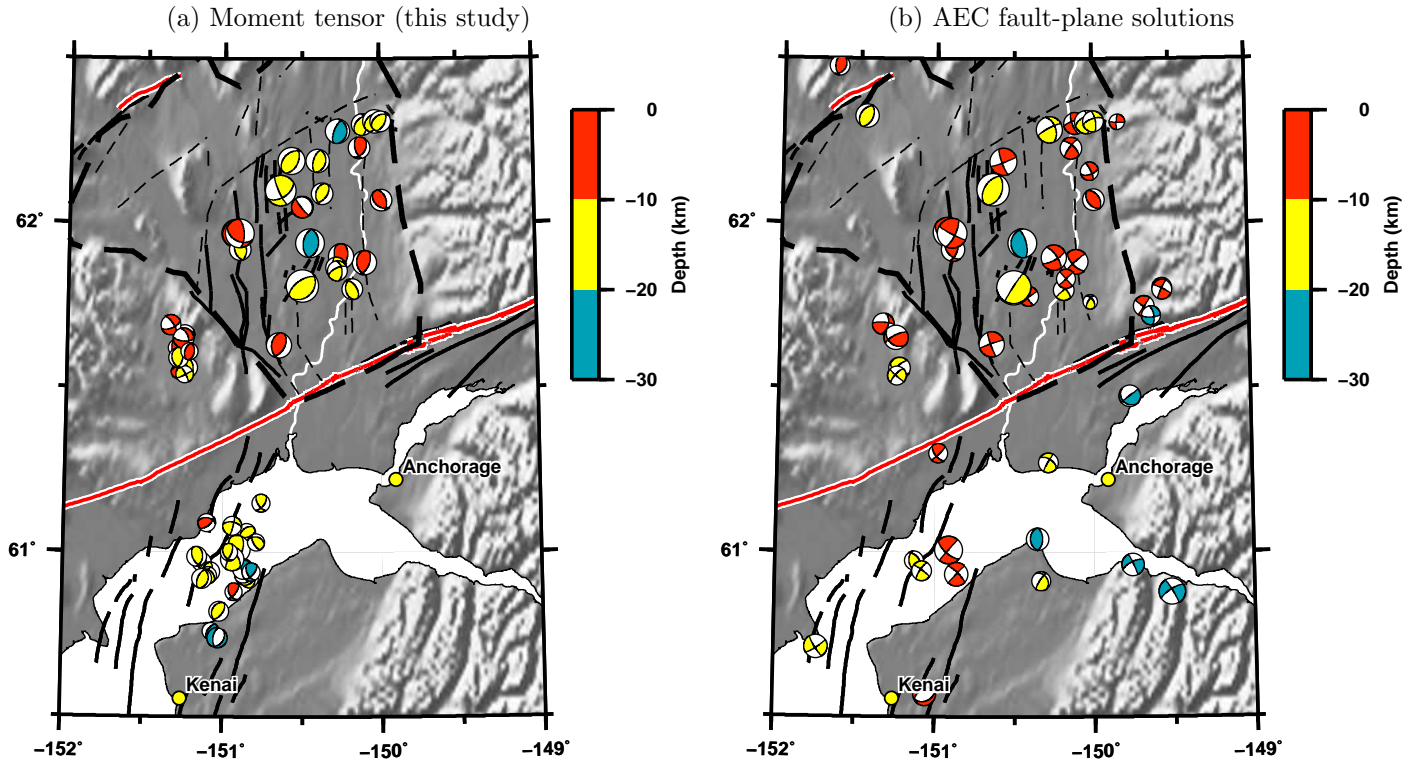


Figure 12: Comparison between moment tensors in this study and an existing catalog. All earthquakes shown are for depth ≤ 30 km and between 2007-08-15 to 2017-01-01. (a) Moment tensors estimated in this study: 53 total, 26 of which are in (b), 27 which are new. These mechanisms are estimated from waveforms and first-motion polarities. (b) Moment tensors in the Alaska Earthquake Center fault-plane catalog: 46 total, 26 of which are in (a), 20 of which we do not examine. These mechanisms are estimated from first-motion polarities.

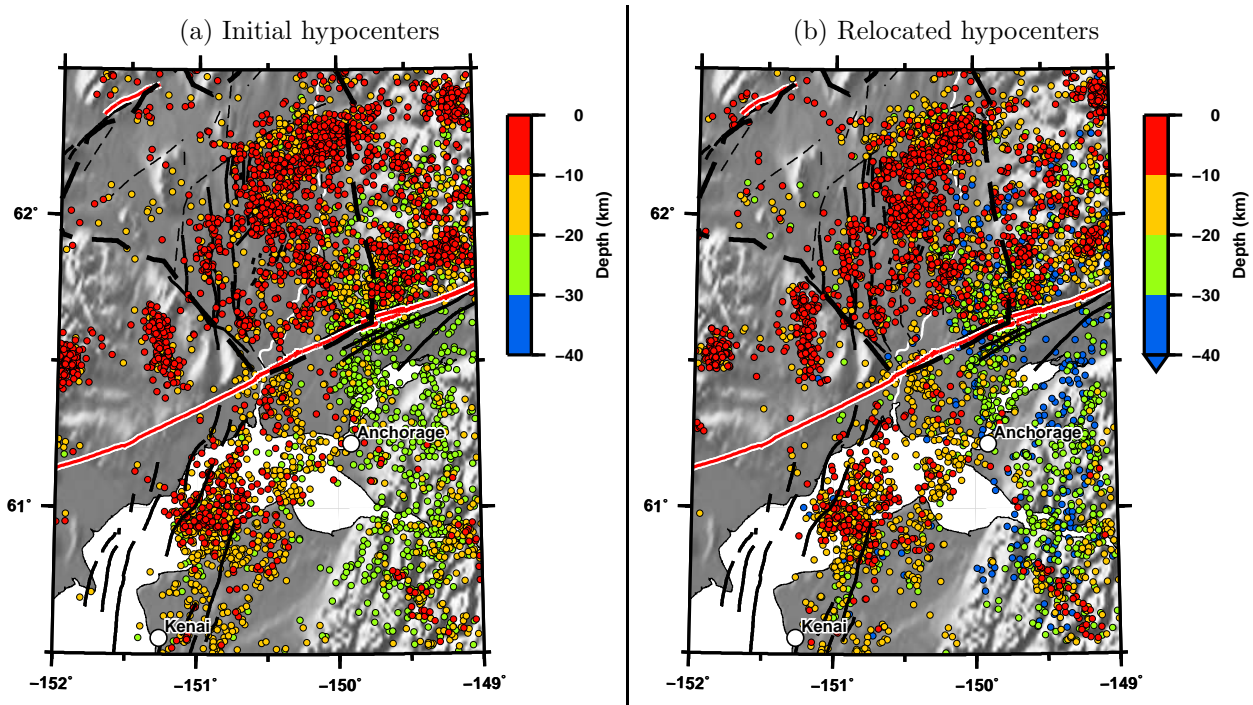


Figure 13: Relocation of hypocenters using a double-difference approach. The crustal earthquakes considered have depth ≤ 30 km, $M_w \geq 1.5$, and occurred between 1990-01-01 and 2017-01-01. See Section 4 and Figure S14 for details.

735 **Appendix A. Summary of felt reports for 1933, 1943, and 1954 earthquakes**

736 Here we summarize the entries for the 1933, 1943, and 1954 earthquakes within the annual earthquake
737 volumes of the U.S. Coast and Geodetic Survey [106, 107, 108]. See felt report locations on maps in
738 Figure S15.

739 *1933-04-27 M_w 6.8*

740 The complete entry in [106]:

741 *April 26:* 16:36*. Instrumental epicenter 62° north, 151° west. Anchorage, VI. Telegraph lines
742 were down for a distance of 50 miles from Anchorage. The shock lasted about 3 minutes. Plate
743 glass windows in several stores were broken and stocks of good tumbled from their shelves. This
744 earthquake was considered by residents as the worst in 30 years.

745 The quake was felt strongly on Kodiak Island and along the Aleutian Islands. It was felt strongly
746 at Curry, McGrath, Seward, and Wasilla; Dillingham (Kanakanak), IV; reported light at Healy.
747 The shock was felt at College, Fairbanks, Susitna, Valdez, and Whale Island.

748 Because of the difficulty in correlating the times of occurrence of the following aftershocks it has
749 been considered best to list them all as individual shocks, even though it is evident that this is
750 not always true.

751 *April 26:* Homer; earthquake and following tremors.

752 *April 26:* Kasilof;

753 *April 26:* Big Susitna River District, VII.

754 *April 26:* Old Tyonek, VII. Houses shaken off foundations.

755 *1943-11-03 M_w 7.3*

756 The complete entry in [107]:

757 **November 3:** 04:32.3.* Anchorage. Sharp shock with abrupt heaving motion made doors swing
758 and windows rattle. Generally felt. A light after-shock occurred at 05:40. Several slight tremors
759 were felt at intervals until about 07:30. Pen on recording rain gage made mark about $\frac{3}{4}$ inch
760 wide at time of main shock. Similar marks were recorded on the barograph traces. Epicenter
761 probably near 62° north, 151° west.

762 Felt at McGrath 04:33. Slight shock reported by Weather Bureau Observer as continuing for
763 about fifteen seconds. "Wall clocks in the Civil Aeronautics Administration and Weather Bureau
764 Offices were stopped. The barograph trace showed no indication of the quake ..." "

765 Felt at Bethel 04:37. Tremors lasting 20 seconds were felt by several. Faint rumbling underground
766 and moderately loud cracking of ice was heard. Building swayed. “The noise moved down the
767 river quickly and then seemed to pass under the station making the earth tremble comparable
768 to a locomotive passing. The ice in the river made a cracking noise for about an hour after the
769 tremors, which lasted about 20 seconds.”

770 Following [107], [55] lists only three felt reports (Anchorage, McGrath, and Bethel), but we found 10
771 additional felt reports within the monthly weather records. Furthermore, p. 4 of the 1943-11-03 Fairbanks
772 Daily News-Miner had an article headlined “Big Quake Felt Here This Morn”. We speculate that the
773 shortage of reports in [107] was due to the national focus on WWII, which may have limited other duties
774 such as earthquake compilations.

775 1954-10-03 M_w 6.4

776 The complete entry in [108]:

777 **October 3:** 01:18:46*. Epicenter $60\frac{1}{2}^\circ$ north, 151° west, Kenai Peninsula, W. VIII. A sharp
778 earthquake rocked a 1,000 square mile area of the lower Alaska mainland. Concrete walls cracked;
779 plaster showered down; plate glass windows shattered; merchandise toppled from shelves at An-
780 chorage, Homer, Kenai, Seward, Sterling, and Valdez. Minor landslides spilled down on the
781 Seward-Anchorage highway. More than 140 feet of railroad tracks were knocked out of commis-
782 sion just north of Potter. Residents on top floors in Anchorage’s two 14-story “skyscrapers” fled
783 into the streets when the violent rocking broke water connections. At the Denali Theater, where
784 a midnight show was in progress, some 850 patrons rushed toward the exists [sic], climbing over
785 seats in a frenzy to escape. Three persons were reported injured slightly in the rush. Motorists
786 driving cars at the time of the quake said it felt “like moving along on a flat tire.” It was also
787 felt at Cordova, Eklutna, Fairbanks, Kaslof, Kodiak, Latouche, Mantanuska [sic] Agricultural
788 Experiment Station, Moose Pass (severe enough to shake things from the shelves), Palmer, Pun-
789 tillia, and Yakutat. Five aftershocks of a few seconds duration followed the main quake at 02:43,
790 05:21, 05:34, 06:18, and 07:26.

791 The MMI VIII shaking intensity for the 1954 M_w 6.4 earthquake was the largest ever reported on the western
792 Kenai Peninsula (Homer, Kenai, Sterling)—even exceeding the MMI VII of the 1964 M_w 9.2 earthquake [55].